Supporting Information

Fine-tuning Central Extended Unit Symmetry via An Atom-Level Asymmetric Molecular Design Enables Efficient Binary Organic Solar Cells

Jian Liu [a†], Ruohan Wang [a†], Longyu Li [a], Wenkai Zhao [b], Zhaochen Suo [a], Wendi Shi [a], Guankui Long [b], Zhaoyang Yao [a], Xiangjian Wan*[a], Yongsheng Chen*[a]

[a] State Key Laboratory of Elemento-Organic Chemistry, Frontiers Science Center for New Organic Matter, The Centre of Nanoscale Science and Technology and Key Laboratory of Functional Polymer Materials, Institute of Polymer Chemistry, Renewable Energy Conversion and Storage Center (RECAST), Tianjin Key Laboratory of functional polymer materials, Nankai University, Tianjin, 300071, China.

E-mail: xjwan@nankai.edu.cn, yschen99@nankai.edu.cn.

[b] School of Materials Science and Engineering, National Institute for Advanced Materials, Renewable Energy Conversion and Storage Center (RECAST), Nankai University, Tianjin, 300350, China.

† These authors contributed equally.

Experimental section

Materials and Synthesis.

Starting material such as compound **1**, compound **4**, iodine pentoxide, phosphorus oxychloride, boron trifluoride diethyl etherate and boron tribromide were purchased from *Energy Chemical*. *N*-ethyl-*N*-isopropylpropan-2-amine and 1-bromopyrrolidine-2,5-dione were purchased from TCI. Polymer donor PM6 and 2-(5,6-difluoro-3-oxo-2,3-dihydro-1H-inden-1-ylidene) malononitrile were purchased from Solarmer Material (Beijing) Inc and Woerjiming (Beijing) Technology Development Institute. All chemicals and other regents, unless otherwise specified, were purchased from commercial suppliers and were directly used without further purification. Compound 1A and compound 5 was synthesized according to literature procedure[1, 2]. The target acceptors CH-PHE, CH-Bzq and CH-Bzq-Br were synthetized according to the following steps, respectively.

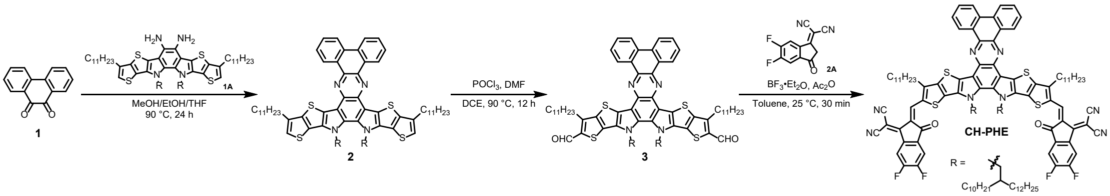

Scheme S1. The synthetic route of CH-PHE.

Synthesis of Compound 2

A solution of compound 1A (500 mg, 0.36 mmol, 1.00 eq) in tetrahydrofuran (12.0 mL) was added to a suspension of compound 1 (112 mg, 0.54 mmol, 1.50 eq) in methanol (12.0 mL) and ethanol (12.0 mL). Then the reaction mixture was stirred at 90 °C for 24 h under argon atmosphere. After reaction, the reaction mixture was quenched with water (50 mL) and then extracted with dichloromethane (3 × 50 mL). The organic phase was washed with brine (3 × 150 mL), dried with anhydrous sodium sulfate, filtered and concentrated under reduced pressure to give a residue. The crude product was purified by silica gel column chromatography (petroleum ether/dichloromethane = 8/1) to afford compound 2 as a red solid (420 mg, 0.27 mmol, 74.75% yield).

^{1}H NMR (400 MHz, $CDCl_3$) δ 9.74 (d, J = 7.7 Hz, 2H), 8.68 (d, J = 8.1 Hz, 2H), 7.90 (t, J = 7.5 Hz, 2H), 7.81 (t, J = 7.2 Hz, 2H), 7.02 (s, 2H), 4.68 (d, J = 7.5 Hz, 4H), 2.92 (t, J = 7.5 Hz, 4H), 2.23-2.08 (m, 2H), 2.02-1.84 (m, 4H), 1.58-1.47 (m, 6H), 1.43 (dt, J = 14.2, 6.8 Hz, 4H), 1.39-1.20 (m, 30H), 1.15 (dd, J = 14.7, 8.4 Hz, 14H), 1.04 (d, J = 21.8 Hz, 22H), 1.01-0.83 (m, 44H), 0.80 (dd, J = 13.0, 6.0 Hz, 10H).

^{13}C NMR (101 MHz, $CDCl_3$) δ 143.4, 139.1, 137.5, 137.1, 135.9, 131.4, 131.4, 131.2, 129.1, 127.8, 126.1, 123.8, 123.0, 122.9, 118.8, 118.0, 55.3, 38.8, 32.1, 32.1, 30.7, 30.0, 29.9, 29.9, 29.8, 29.8, 29.8, 29.7, 29.6, 29.6, 29.6, 29.5, 29.1, 25.8, 22.9, 22.9, 14.3, 14.3.

Synthesis of Compound 3

To a flask was added compound 2 (420 mg, 0.27 mmol, 1.00 eq) and anhydrous 1,2-dichloroethane (30.0 mL) at 0 °C. The solution was degassed and purged with argon for three times, then DMF (5.00 mL) was added dropwise to the reaction mixture, followed by $POCl_3$ (2.00 mL). After addition, the reaction mixture was stirred at 90 °C for 12 h under argon atmosphere. The reaction mixture was neutralized with saturated sodium acetate for 6 h and then extracted with dichloromethane (3 × 40 mL). The organic phase was washed with brine (3 × 90 mL), dried with anhydrous sodium sulfate, filtered and concentrated under reduced pressure to give a residue. The crude product was purified by silica gel column chromatography (petroleum ether/dichloromethane = 2/1) to afford compound 3 as a red solid (316 mg, 0.19 mmol, 72.64% yield).

^{1}H NMR (400 MHz, $CDCl_3$) δ 10.16 (s, 2H), 9.69 (dd, *J* = 7.9, 1.0 Hz, 2H), 8.70 (d, *J* = 8.0 Hz, 2H), 7.92 (t, *J* = 7.3 Hz, 2H), 7.88-7.82 (m, 2H), 4.70 (d, *J* = 7.6 Hz, 4H), 3.30 (t, *J* = 7.6 Hz, 4H), 2.14 (dd, *J* = 14.9, 10.3 Hz, 2H), 2.07-1.95 (m, 4H), 1.59-1.49 (m, 6H), 1.48-1.39 (m, 4H), 1.38-1.19 (m, 28H), 1.19-1.09 (m, 14H), 1.05 (m, 22H), 1.01-0.86 (m, 34H), 0.86-0.81 (m, 14H), 0.78 (t, *J* = 7.1 Hz, 8H).

^{13}C NMR (101 MHz, $CDCl_3$) δ 181.8, 147.0, 144.4, 139.8, 137.2, 136.9, 135.9, 132.5, 131.5, 130.6, 129.9, 129.5, 127.9, 127.4, 126.0, 122.9, 118.8, 55.5, 39.1, 32.1, 32.0, 30.9, 30.6, 29.9, 29.8, 29.8, 29.7, 29.7, 29.7, 29.6, 29.5, 29.5, 29.4, 28.3, 25.7, 22.8, 22.8, 14.3, 14.2.

Synthesis of CH-PHE

Compound 3 (316 mg, 0.19 mmol, 1.00 eq) and compound 2A (131 mg, 0.57 mmol, 3.00 eq) was dissolved in toluene (30.0 mL). The reaction mixture was stirred at 25 °C, then acetic anhydride (1.50 mL) was added dropwise to the reaction mixture, followed by boron trifluoride diethyl etherate (1.00 mL). After addition, the reaction mixture was stirred at 25 °C for 30 min and then quenched with saturated sodium carbonate aqueous solution (30 mL). The mixture was extracted with ethyl acetate (1 × 40 mL) and chloroform (3 × 30 mL). The organic phase was washed with brine (3 × 120 mL), dried with anhydrous sodium sulfate, filtered and concentrated under reduced pressure to give a residue. The crude product was purified by silica gel column chromatography (petroleum ether/chloroform = 1/2) to afford CH-PHE as a dark black solid (256 mg, 0.12 mmol, 64.19% yield).

^{1}H NMR (400 MHz, $CDCl_3$) δ 9.53 (dd, *J* = 18.0, 8.7 Hz, 2H), 9.19-9.00 (m, 2H), 8.73-8.62 (m, 2H), 8.52-8.29 (m, 2H), 7.96-7.82 (m, 4H), 7.66-7.50 (m, 2H), 4.86 (d, *J* = 6.2 Hz, 4H), 3.37-3.22 (m, 4H), 2.35-2.23 (m, 2H), 1.99-1.87 (m, 4H), 1.62-1.53 (m, 4H), 1.51-1.37 (m, 8H), 1.32 (dd, *J* = 10.0, 5.4 Hz, 6H), 1.19 (ddd, *J* = 16.7, 15.5, 9.4 Hz, 30H), 1.12-0.87 (m, 62H), 0.86-0.77 (m, 14H), 0.74 (t, *J* = 7.0 Hz, 6H).

^{13}C NMR (101 MHz, $CDCl_3$) δ 185.9, 157.9, 155.5, 155.4, 154.1, 152.9, 152.8, 146.6, 140.0, 138.4, 136.3, 136.0, 134.9, 134.1, 133.5, 133.4, 131.6, 131.0, 130.2, 130.0, 128.3, 125.9, 123.3, 120.2, 119.3, 114.8, 114.7, 114.5, 114.3, 112.2, 112.0, 67.9, 55.9, 39.6, 32.1, 31.7, 30.7, 30.3, 30.0, 29.9, 29.9, 29.8, 29.8, 29.6, 29.5, 26.0, 22.8, 22.8, 14.2, 14.2, 14.2.

HRMS (m/z, MALDI): calculated for $C_{128}H_{158}F_4N_8O_2S_4$ $[M]^+$: 2044.1360; found: 2044.1343.

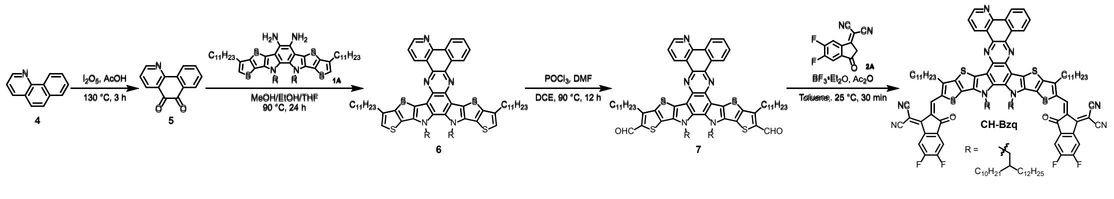

Scheme S2. The synthetic route of CH-Bzq.

Synthesis of Compound 5

Compound 4 (6.4 g, 35.74 mmol, 1.00 eq) and 1,5-diiodopentaoxidane (15.51 g, 46.46 mmol, 1.30 eq) were added to a 250 mL round-bottom flask with glacial acetic acid (100 mL). The orange mixture was stirred at 130 °C for 3 h under air, resulting in a dark purple solution. After reaction, the mixture was poured into 200 mL distilled water and then stand overnight at room temperature. The precipitate was isolated by vacuum filtration and subsequently dissolved in dichloromethane (150 mL) to give a dark red solution, then the solution was washed with saturated sodium carbonate aqueous solution (3 × 100 mL) and saturated sodium thiosulfate solution (3 × 100 mL). The organic phase was dried with anhydrous sodium sulfate, filtered and concentrated under reduced pressure to afford compound 5 as a yellow solid (5.5 g, 26.31 mmol, 73.61% yield).

^{1}H NMR (400 MHz, $CDCl_3$) δ 8.88 (dd, J = 4.7, 1.8 Hz, 1H), 8.68 (dd, J = 7.9, 0.9 Hz, 1H), 8.39 (dd, J = 7.9, 1.8 Hz, 1H), 8.18 (dd, J = 7.8, 1.2 Hz, 1H), 7.79 (td, J = 7.7, 1.3 Hz, 1H), 7.57 (td, J = 7.6, 1.1 Hz, 1H), 7.41 (dd, J = 7.9, 4.7 Hz, 1H).

^{13}C NMR (101 MHz, $CDCl_3$) δ 179.8, 179.0, 155.4, 153.5, 137.0, 136.4, 136.3, 131.4, 131.2, 129.9, 126.7, 126.3, 124.3.

Synthesis of Compound 6

A solution of compound 1A (500 mg, 0.36 mmol, 1.00 eq) in tetrahydrofuran (12.0 mL) was added to a suspension of compound 5 (113 mg, 0.54 mmol, 1.50 eq) in methanol (12.0 mL) and ethanol (12.0 mL). Then the reaction mixture was stirred at 90 °C for 24 h under argon atmosphere. After reaction, the reaction mixture was quenched with water (50 mL) and then extracted with dichloromethane (3 × 50 mL). The organic phase was washed with brine (3 × 150 mL), dried with anhydrous sodium sulfate, filtered and concentrated under reduced pressure to give a residue. The crude product was purified by silica gel column chromatography (petroleum ether/dichloromethane = 1/1) to afford compound 6 as a red solid (422 mg, 0.27 mmol, 75.06% yield).

^{1}H NMR (400 MHz, $CDCl_3$) δ 9.95 (s, 1H), 9.69 (d, J = 7.7 Hz, 1H), 9.36 (s, 1H), 9.14 (s, 1H), 8.06-7.99 (m, 1H), 7.90 (dd, J = 18.7, 11.5 Hz, 2H), 7.04 (s, 2H), 4.69 (d, J = 7.8 Hz, 4H), 2.99-2.85 (m, 4H), 2.22-2.09 (m, 2H), 1.92 (dd, J = 13.6, 7.2 Hz, 4H), 1.52 (m, 6H), 1.47-1.39 (m, 4H), 1.38-1.20 (m, 30H), 1.19-1.12 (m, 12H), 1.06 (m, 22H), 0.98-0.69 (m, 56H).

^{13}C NMR (151 MHz, $CDCl_3$) δ 150.4, 148.1, 143.5, 143.3, 139.1, 138.0, 137.6, 137.1, 137.0, 136.3, 136.0, 133.6, 132.4, 132.3, 131.6, 131.5, 129.5, 129.3, 126.3, 125.3, 124.9, 123.8, 123.7, 123.0, 122.8, 122.8, 119.0, 119.0, 117.9, 117.8, 55.3, 38.8, 32.1, 32.1, 32.1, 30.7, 29.9, 29.9, 29.8, 29.8, 29.8, 29.7, 29.6, 29.6, 29.6, 29.5, 29.1, 25.8, 22.9, 22.8, 14.3, 14.3.

Synthesis of Compound 7

To a flask was added compound 6 (422 mg, 0.27 mmol, 1.00 eq) and anhydrous 1,2-dichloroethane (30.0 mL) at 0 °C. The solution was degassed and purged with argon for three times, then DMF (5.00 mL) was added dropwise to the reaction mixture, followed by $POCl_3$ (2.00 mL). After addition, the reaction mixture was stirred at 90 °C for 12 h under argon atmosphere. The reaction mixture was neutralized with saturated sodium acetate for 6 h and then extracted with dichloromethane (3 × 40 mL). The organic phase was washed with brine (3 × 90 mL), dried with anhydrous sodium sulfate, filtered and concentrated under reduced pressure to give a residue. The crude product was purified by silica gel column chromatography (petroleum ether/dichloromethane = 1/1) to afford compound 7 as a red solid (325 mg, 0.20 mmol, 74.35% yield).

^{1}H NMR (400 MHz, $CDCl_3$) δ 10.17 (s, 2H), 9.85 (d, J = 7.7 Hz, 1H), 9.63 (d, J = 7.9 Hz, 1H), 9.35 (d, J = 7.1 Hz, 1H), 9.15 (d, J = 3.5 Hz, 1H), 8.02 (t, J = 7.5 Hz, 1H), 7.93 (t, J = 7.5 Hz, 1H), 7.84 (dd, J = 7.7, 4.5 Hz, 1H), 4.71 (d, J = 7.5 Hz, 4H), 3.30 (dd, J = 10.0, 7.6 Hz, 4H), 2.17-2.09 (m, 2H), 2.00 (m, 4H), 1.58-1.51 (m, 6H), 1.42 (d, J = 6.5 Hz, 4H), 1.23 (m, J = 10.6 Hz, 30H), 1.13 (m, J = 6.5 Hz, 12H), 1.05 (m, 22H), 0.95-0.88 (m, 26H), 0.86-0.80 (m, 20H), 0.78 (t, J = 7.1 Hz, 10H).

^{13}C NMR (101 MHz, $CDCl_3$) δ 181.9, 181.8, 150.8, 148.1, 147.1, 146.9, 144.5, 144.3, 139.7, 138.7, 137.3, 137.3, 137.0, 137.0, 136.4, 136.0, 133.5, 132.7, 132.6, 132.5, 131.9, 129.9, 129.8, 129.8, 129.5, 127.7, 127.5, 125.8, 125.2, 125.0, 122.9, 118.7, 118.6, 55.6, 39.1, 32.0, 32.0, 30.9, 30.7, 29.9, 29.8, 29.8, 29.8, 29.7, 29.7, 29.7, 29.6, 29.5, 29.5, 29.4, 28.3, 25.8, 22.8, 22.8, 14.2, 14.2, 14.2.

Synthesis of CH-Bzq

Compound 7 (325 mg, 0.20 mmol, 1.00 eq) and compound 2A (139 mg, 0.60 mmol, 3.00 eq) was dissolved in toluene (30.0 mL). The reaction mixture was stirred at 25 °C, then acetic anhydride (1.50 mL) was added dropwise to the reaction mixture, followed by boron trifluoride diethyl etherate (1.00 mL). After addition, the reaction mixture was stirred at 25 °C for 30 min and then quenched with saturated sodium carbonate aqueous solution (30 mL). The mixture was extracted with ethyl acetate (1 × 40 mL) and chloroform (3 × 30 mL). The organic phase was washed with brine (3 × 120 mL), dried with anhydrous sodium sulfate, filtered and concentrated under reduced pressure to give a residue. The crude product was purified by silica gel column chromatography (petroleum ether/chloroform = 1/6) to afford CH-Bzq as a dark black solid (307 mg, 0.15 mmol, 74.87% yield).

^{1}H NMR (400 MHz, $CDCl_3$) δ 9.61 (d, J = 7.2 Hz, 1H), 9.28 (dd, J = 10.4, 6.3 Hz, 2H), 9.12-9.03 (m, 3H), 8.39 (ddd, J = 20.9, 9.7, 6.5 Hz, 2H), 7.91-7.82 (m, 2H), 7.77

(d, *J* = 2.0 Hz, 1H), 7.65 (dd, *J* = 11.2, 7.3 Hz, 2H), 4.90 (d, *J* = 7.3 Hz, 4H), 3.25 (dd, *J* = 16.0, 8.5 Hz, 4H), 2.31 (d, *J* = 9.5 Hz, 2H), 1.94-1.84 (m, 4H), 1.53 (dt, *J* = 14.3, 7.2 Hz, 6H), 1.38 (m, *J* = 4.5 Hz, 4H), 1.29 (m, 10H), 1.26-1.16 (m, 28H), 1.08-0.89 (m, 62H), 0.84-0.78 (m, 12H), 0.74 (dd, *J* = 14.0, 7.2 Hz, 8H).

^{13}C NMR (101 MHz, CDCl$_3$) δ 186.1, 158.1, 157.9, 157.8, 155.6, 155.5, 154.0, 153.9, 153.0, 152.9, 146.7, 146.7, 146.6, 146.6, 139.8, 138.8, 138.4, 136.4, 136.3, 136.3, 136.1, 134.8, 134.3, 133.5, 133.5, 133.4, 133.4, 133.4, 131.1, 130.8, 130.8, 130.1, 129.7, 125.1, 124.9, 122.9, 120.0, 119.9, 119.5, 119.4, 114.9, 114.8, 114.4, 114.3, 112.4, 112.2, 68.2, 68.1, 56.0, 39.8, 32.1, 31.8, 30.8, 30.3, 30.0, 29.9, 29.8, 29.8, 29.8, 29.5, 26.1, 22.8, 14.2, 14.2.

HRMS (m/z, MALDI): calculated for $C_{127}H_{157}F_4N_9O_2S_4$ [M]$^+$: 2046.1386; found: 2046.1375.

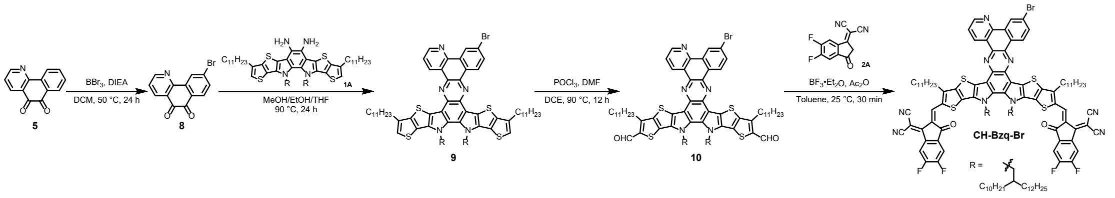

Scheme S3. The synthetic route of CH-Bzq-Br.

Synthesis of Compound 8

To a flask was added compound 5 (628 mg, 3.00 mmol, 1.00 eq) and anhydrous dichloromethane (30,0 mL) at 0 °C. The solution was degassed and purged with argon for three times, then *N*-ethyl-*N*-isopropylpropan-2-amine (388 mg, 3.00 mmol, 1.00 eq) was added dropwise to the reaction mixture, followed by boron tribromide (2.0 M in dichloromethane, 6.00 mL, 12.0 mmol). After addition, the reaction mixture was stirred at 50 °C for 24 h under argon atmosphere. The reaction mixture was quenched with saturated sodium carbonate aqueous solution (30 mL) and extracted with dichloromethane (3 × 30 mL). The organic phase was washed with brine (3 × 120 mL), dried with anhydrous sodium sulfate, filtered and concentrated under reduced pressure to give a residue. The crude product was purified by silica gel column chromatography (petroleum ether/dichloromethane = 1/4) to afford compound 8 as a yellow solid (350 mg, 1.22 mmol, 40.60% yield).

^{1}H NMR (400 MHz, CDCl$_3$) δ 8.89 (dd, *J* = 4.6, 1.5 Hz, 1H), 8.87 (d, *J* = 1.6 Hz, 1H), 8.41 (dd, *J* = 7.7, 1.5 Hz, 1H), 8.04 (d, *J* = 8.3 Hz, 1H), 7.71 (dd, *J* = 8.3, 1.7 Hz, 1H), 7.46 (dd, *J* = 7.8, 4.7 Hz, 1H).

^{13}C NMR (101 MHz, CDCl$_3$) δ 179.2, 178.3, 155.5, 152.3, 137.7, 137.3, 134.4, 132.6, 131.3, 130.1, 129.6, 127.1, 124.9.

HRMS (m/z, ESI): calculated for $C_{13}H_6BrNO_2$ [M+Na]$^+$: 309.9475; found: 309.9474.

Synthesis of Compound 9

A solution of compound 1A (500 mg, 0.36 mmol, 1.00 eq) in tetrahydrofuran (12.0

mL) was added to a suspension of compound 8 (155 mg, 0.54 mmol, 1.50 eq) in methanol (12.0 mL) and ethanol (12.0 mL). Then the reaction mixture was stirred at 90 °C for 24 h under argon atmosphere. After reaction, the reaction mixture was quenched with water (50 mL) and then extracted with dichloromethane (3 × 50 mL). The organic phase was washed with brine (3 × 150 mL), dried with anhydrous sodium sulfate, filtered and concentrated under reduced pressure to give a residue. The crude product was purified by silica gel column chromatography (petroleum ether/dichloromethane = 2/1) to afford compound 9 as a red solid (477 mg, 0.29 mmol, 80.82% yield).

^{1}H NMR (400 MHz, $CDCl_3$) δ 9.88 (dd, *J* = 8.1, 1.4 Hz, 1H), 9.52 (d, *J* = 8.6 Hz, 1H), 9.48 (d, *J* = 1.8 Hz, 1H), 9.10 (dd, *J* = 4.3, 1.5 Hz, 1H), 8.09 (dd, *J* = 8.5, 1.9 Hz, 1H), 7.84 (dd, *J* = 8.0, 4.4 Hz, 1H), 7.04 (s, 2H), 4.68 (d, *J* = 7.7 Hz, 4H), 2.99-2.82 (m, 4H), 2.24-2.09 (m, 2H), 1.99-1.84 (m, 4H), 1.47-1.39 (m, 4H), 1.38-1.19 (m, 30H), 1.15 (dd, *J* = 11.8, 5.3 Hz, 12H), 1.06 (m, 24H), 0.99-0.83 (m, 46H), 0.80 (dd, *J* = 13.3, 6.3 Hz, 14H).

^{13}C NMR (101 MHz, $CDCl_3$) δ 150.3, 146.6, 143.5, 143.4, 138.2, 137.6, 137.0, 137.0, 136.3, 136.1, 133.6, 133.3, 132.4, 131.5, 131.4, 130.9, 127.5, 127.0, 126.5, 124.3, 123.7, 123.2, 123.0, 122.8, 119.0, 118.9, 117.8, 117.7, 55.4, 38.9, 32.1, 32.1, 32.1, 30.7, 30.0, 29.9, 29.9, 29.8, 29.8, 29.7, 29.6, 29.6, 29.6, 29.5, 29.1, 29.0, 25.9, 22.9, 22.9, 14.3, 14.3.

Synthesis of Compound 10

To a flask was added compound 9 (477 mg, 0.29 mmol, 1.00 eq) and anhydrous 1,2-dichloroethane (30.0 mL) at 0 °C. The solution was degassed and purged with argon for three times, then DMF (5.00 mL) was added dropwise to the reaction mixture, followed by $POCl_3$ (2.00 mL). After addition, the reaction mixture was stirred at 90 °C for 12 h under argon atmosphere. The reaction mixture was neutralized with saturated sodium acetate for 6 h and then extracted with dichloromethane (3 × 40 mL). The organic phase was washed with brine (3 × 90 mL), dried with anhydrous sodium sulfate, filtered and concentrated under reduced pressure to give a residue. The crude product was purified by silica gel column chromatography (petroleum ether/dichloromethane = 1/1) to afford compound 10 as a red solid (391 mg, 0.23 mmol, 79.27% yield).

^{1}H NMR (400 MHz, $CDCl_3$) δ 10.17 (d, *J* = 1.2 Hz, 2H), 9.82 (dd, *J* = 8.1, 1.6 Hz, 1H), 9.49 (d, *J* = 2.0 Hz, 1H), 9.46 (d, *J* = 8.6 Hz, 1H), 9.13 (dd, *J* = 4.4, 1.7 Hz, 1H), 8.10 (dd, *J* = 8.6, 2.0 Hz, 1H), 7.85 (dd, *J* = 8.1, 4.5 Hz, 1H), 4.71 (d, *J* = 7.7 Hz, 4H), 3.29 (t, *J* = 6.9 Hz, 4H), 2.14 (dd, *J* = 10.6, 5.3 Hz, 2H), 2.00 (dt, *J* = 14.9, 7.4 Hz, 4H), 1.57 (dd, *J* = 13.5, 6.2 Hz, 4H), 1.48-1.39 (m, 4H), 1.38-1.18 (m, 32H), 1.13 (dd, *J* = 13.4, 6.4 Hz, 12H), 1.07 (m, *J* = 15.3 Hz, 22H), 0.99-0.87 (m, 34H), 0.86-0.81 (m, 14H), 0.78 (t, *J* = 7.2 Hz, 8H).

^{13}C NMR (101 MHz, $CDCl_3$) δ 181.8, 150.6, 146.9, 146.8, 146.3, 144.5, 144.4, 138.5, 137.9, 137.3, 137.3, 137.0, 136.1, 135.9, 133.4, 132.9, 132.4, 132.4, 132.3, 130.1, 129.7, 129.7, 127.5, 127.4, 127.4, 126.5, 125.7, 124.7, 123.0, 118.6, 118.5, 55.6, 39.2, 32.0, 32.0, 32.0, 31.0, 30.7, 29.9, 29.9, 29.8, 29.8, 29.7, 29.5, 29.5, 29.4, 29.4, 28.3, 25.9, 22.8, 22.8, 22.7, 14.2, 14.2.

Synthesis of CH-Bzq-Br

Compound 10 (391 mg, 0.23 mmol, 1.00 eq) and compound 2A (159 mg, 0.69 mmol, 3.00 eq) was dissolved in toluene (30.0 mL). The reaction mixture was stirred at 25 °C, then acetic anhydride (1.50 mL) was added dropwise to the reaction mixture, followed by boron trifluoride diethyl etherate (1.00 mL). After addition, the reaction mixture was stirred at 25 °C for 30 min and then quenched with saturated sodium carbonate aqueous solution (30 mL). The mixture was extracted with ethyl acetate (1 × 40 mL) and chloroform (3 × 30 mL). The organic phase was washed with brine (3 × 120 mL), dried with anhydrous sodium sulfate, filtered and concentrated under reduced pressure to give a residue. The crude product was purified by silica gel column chromatography (petroleum ether/chloroform = 1/4) to afford CH-Bzq-Br as a dark black solid (385 mg, 0.18 mmol, 78.79% yield).

^{1}H NMR (400 MHz, $CDCl_3$) δ 9.43 (d, J = 8.0 Hz, 1H), 9.22 (d, J = 1.2 Hz, 1H), 9.10 (s, 1H), 9.05 (s, 1H), 9.01 (dd, J = 4.2, 1.5 Hz, 1H), 8.96 (d, J = 8.4 Hz, 1H), 8.46 (dd, J = 9.8, 6.5 Hz, 1H), 8.39 (dd, J = 9.8, 6.5 Hz, 1H), 7.82 (dd, J = 8.7, 1.0 Hz, 1H), 7.74-7.68 (m, 2H), 7.68-7.62 (m, 1H), 4.91 (d, J = 7.7 Hz, 4H), 3.26 (t, J = 7.5 Hz, 2H), 3.19 (t, J = 6.4 Hz, 2H), 2.37-2.26 (m, 2H), 1.96-1.79 (m, 4H), 1.43-1.27 (m, 14H), 1.27-1.12 (m, 34H), 1.12-0.91 (m, 64H), 0.80 (dt, J = 12.7, 6.9 Hz, 12H), 0.73 (t, J = 7.0 Hz, 6H).

^{13}C NMR (101 MHz, $CDCl_3$) δ 186.1, 186.1, 158.0, 157.8, 155.6, 153.9, 153.8, 153.2, 153.1, 153.1, 153.0, 152.9, 151.0, 146.7, 146.7, 146.2, 138.8, 138.4, 138.3, 136.4, 136.3, 136.3, 136.2, 134.9, 134.8, 134.4, 134.3, 134.3, 133.3, 133.3, 133.2, 132.7, 132.3, 131.1, 131.0, 129.4, 127.5, 126.0, 125.2, 125.2, 123.1, 119.8, 119.8, 119.5, 119.4, 115.0, 114.9, 114.8, 114.6, 114.4, 114.4, 112.7, 112.5, 112.4, 68.4, 56.1, 40.0, 32.1, 31.9, 31.9, 31.1, 30.4, 30.0, 29.9, 29.8, 29.5, 29.5, 26.3, 22.8, 14.2, 14.2.

HRMS (m/z, MALDI): calculated for $C_{127}H_{156}BrF_4N_9O_2S_4$ $[M]^+$: 2123.0418; found: 2125.0479.

Instruments and Measurements

The Nuclear Magnetic Resonance (NMR) Spectra and High-Resolution Mass Spectra (HRMS).

The ^1H and ^{13}C nuclear magnetic resonance (NMR) spectra of all compounds were obtained from a Bruker AV-400 MHz and AV-600 MHz Spectrometer. Chemical shifts are reported in parts per million (ppm, δ). The High-Resolution Mass Spectra (HRMS) were recorded by Solarix scimax MRMS with high-resolution matrix-assisted laser desorption/ionization (HR-MALDI).

Thermogravimetric Analysis (TGA) Analysis.

The TGA analysis was carried out on a TG209 DSC204 DMA242 TMA202 (NETZSCH) instrument with a heating rate of 5 °C min^{-1} under nitrogen atmosphere.

Density Functional Theory (DFT) Calculation Method.

All the alkyl chains were replaced with methyl groups (-CH_3) to reduce the computational requirements. The structures were subsequently optimized with Density Functional Theory (DFT) in vacuum within the Gaussian 16 software. The energy level and dipole moment of frontier molecular orbital were obtained at the B3LYP/6-31G*level.

Single Crystal Growth and Measurement.

Single crystals of CH-Bzq and CH-Bzq-Br were grown by the liquid diffusion method at room temperature. In detail, 1.5 mL of methanol was transferred to 0.15 mL of concentrated chloroform solution of CH-Bzq and CH-Bzq-Br slowly, and the beautiful cuboid-shape dark purple crystals were formed on the inner glassy tube after about 7 days. The X-ray diffraction signals of single crystal were collected on Rigaku XtalAB PRO MM007 DW. The crystal was kept at 193.0 K during data collection.

UV-visible (UV-vis) Absorption.

The UV-vis spectra were obtained by a Cary 5000 UV-vis spectrophotometer.

Electrochemical Characterizations.

The CV experiments were performed with a LK98B II Microcomputer-based Electrochemical Analyzer. All measurements were conducted at room temperature with a three-electrode configuration. Among them, a glassy carbon electrode was employed as the working electrode, a saturated calomel electrode (SCE) was used as the reference electrode, and a Pt wire was used as the counter electrode. Tetrabutyl ammonium phosphorus hexafluoride (n-Bu_4NPF_6, 0.1 M) in acetonitrile was employed as the supporting electrolyte, and the scan rate was kept at 100 mV s^{-1}. Electrochemically reversible ferrocene was employed as internal reference. The HOMO and LUMO energy levels were calculated from the onset oxidation and the onset reduction potentials, respectively, by following the equation $E_{HOMO} = -(4.80 + E_{ox}^{onset})\ eV$, $E_{LUMO} = -(4.80 + E_{re}^{onset})\ eV$.

Small-area Device Fabrication and Characterization.

The device structure was ITO/2PACZ/Active layer/PNDIT-F3N/Ag. ITO coated glass substrates were cleaned with detergent water, deionized water, acetone and isopropyl alcohol in an ultrasonic bath sequentially for 15 min. Before use, the cleaned ITO substrates were treated with UV exposure for 15 min in a UV-ozone chamber.

2PACZ in ethanol solution was spin-coated on the treated-ITO glass at 3000 rpm for 30 s and then thermal annealing at 100 °C for 20 minutes. After annealing treatment, the substrates were transferred to a glove box filled with nitrogen. A chloroform solution containing the PM6 and acceptors was prepared to spin coating for fabricating active layer, and 1,3,5trichlorobenzene (TCB) was chosen as the additive (10 mg/mL). The total concentration was 13.2 mg/mL and the D/A ratio was kept as 1:1.2. After solution deposition, the active layer was annealed at 100°C for 5 minutes. Then PNDIT-F3N as the electron transporting layer was spin-coated on the active layer by 3000 rpm from methyl alcohol solution (1 mg/mL). Finally, a layer of Ag with thickness of 150 nm was deposited under 2×10^{-6} Pa.

The current density-voltage (*J-V*) measurement of photovoltaic devices were performed by using the solar simulator (SS-F5-3A, Enli Technology, xenon lamp, filter model AMFG2.0) along with AM 1.5G spectra (100 mW cm^{-2}), which was calibrated by a standard Si solar cell (made by Enli Technology Co., Ltd., Taiwan, and calibrated report can be traced to NREL. Device area is approximately 4 mm^2. A mask with 3.24 mm^2 area was used to measure the *J-V* characteristics. The spectral between reference cell and devices could match well during the test (within 5% errors). The current-voltage scan speed and dwell time are 0.02 V/s and 1 ms respectively. No pretreatments (light soaking or holding cell at a bias) were required before *J-V* testing, and all the measurements were conducted in a nitrogen-filled glovebox at room temperature (ca. 25 °C) without attaching any antireflection coating on the incident plane of solar cells. Note that there is no hysteresis or other unusual behaviors during the measurements of solar cells. The EQE spectra were measured by using a QE-R Solar Cell Spectral Response Measurement System (Enli Technology Co., Ltd., Taiwan).

Large-area OSCs Module Fabrication

The OSC modules with the structure glass/ITO/PEDOT:PSS/PM6:CH-Bzq-Br/PNDIT-F3N/Ag were fabricated via blade-coating. The patterned indium tin oxide (ITO)-coated glass substrates were ultrasonically cleaned by using cleaner, deionized water, acetone and isopropanol, followed by oxygen plasma for 15 min. Subsequently, The PEDOT:PSS layer was blade-coated onto the ITO substrate with the gap between the substrate and the blade being 200 μm at a substrate temperature of about 70 °C and then thermally annealed at 150 °C for 20 min. Then, the active layer solution (D:A=1:1.2, 9 mg mL^{-1}:10.8 mg mL^{-1}) was dissolved in o-xylene. The active layer solution was coated onto Glass/ITO/PEDOT:PSS surface in the air at a substrate temperature of 60 °C and a coating speed of 10 mm s^{-1} with the gap between the substrate and the blade being 300 μm. Subsequently, the substrates were transferred to a nitrogen-purged glove box and annealed at 100 °C for 5 min. After that, a PNDIT-F3N layer was deposited via spin coating. The P2 pattern was mechanically scribed by a plastic tweezer. Next, a 150-nm-thick Ag film was thermally evaporated with a mask under a pressure of 3×10^{-4} pa and the P3 line was formed.

As we shown in Figure S42-S43 about module schematic diagram, our modules consist of six interconnected sub-cells to achieve high efficiency. As mentioned above, the P2 patterns were prepared by physical etching and P3 patterns were prepared by mask evaporation. The device area refers to the overlapping region area between silvertop electrode and ITO substrate, was composed of active area and dead area in this work. Generally, light absorption and energy conversion occur in the active area, while interconnecting region was called dead area that no electricity generation. As a result, geometrical fill factor (GFF) was defined as the ratio of active area to the device area in the module. In this work GFF value can be calculated as [(45 mm - 2.6 mm × 5 - 2 mm) × 45 mm]/(45 mm × 45 mm) × 100% = 66.7%.

Fourier-Transform Photocurrent Spectroscopy EQE (FTPS-EQE) and EQE$_{EL}$.

The OSCs used for the FTPS-EQE spectra measurements are the same with those of the *J-V* measurements, with an conventional device architecture of ITO/2PACz/PM6:Acceptors/F3N/Ag. The FTPS-EQE measurement was carried out on an integrated system (PECT-600, Enli Technology Co., Ltd.), where the photocurrent was amplified and modulated by a lock-in instrument. For the EQE$_{EL}$ measurements, a digital source meter (Keithley 2400) was employed to inject electric current into the solar cells, and the emitted photons were collected by a Si diode (Hamamatsu s1337-1010BQ) and indicated by a picometer (Keithley 6482).

Photoluminescent (PL) Measurement.

The steady-state photoluminescence was measured via a FLS1000 equipment. The emission spectra of CH-PHE, CH-Bzq and CH-Bzq-9-Br were recorded by NIR 5509 PMT.

Photocurrent density (J_{ph})-effective voltage (V_{eff}) measurements.

The photocurrent density J_{ph} is defined as $J_{ph} = J_L - J_D$, where J_L and J_D are the photocurrent densities under illumination and in the dark, respectively. The effective voltage V_{eff} is defined as $V_{eff} = V_0 - V_{bias}$, where V_0 is the voltage at which J_{ph} is zero and V_{bias} is the applied external voltage bias. The V_{eff} raises a suitable internal electric field in the device to suppress the charge recombination. In our case, the J_{ph} is saturated at V_{eff} of 1 V. The charge dissociation probability (P(E,T)) was estimated by the value of J_{ph}/J_{sat}, where J_{sat} represents the saturated photocurrent density.

Space-Charge-Limited Current (SCLC) Measurement.

The SCLC method was used to measure the hole and electron mobilities, by using a diode configuration of ITO/2PACz/active layer/MoO$_3$/Ag for hole mobility and ITO/ZnO/active layer/PNDIT-F3N/Ag for electron mobility. The dark current density curves were recorded with a bias voltage in the range of 0~8 V. The mobilities were estimated by taking current-voltage curves and fitting the results based on the equation listed below:

$$J = \frac{9\varepsilon_0\varepsilon_r\mu V^2}{8L^3}$$

where J is the current density, ε_0 is the vacuum permittivity, ε_r is the relative dielectric constant, μ is the mobility, and L is the film thickness. V (V_{app}-V_{bis}) is the internal voltage in the device, where V_{app} is the applied voltage to the device and V_{bis} is the built-in voltage due to the relative work function difference between the two electrodes.

Grazing incidence wide angle X-ray scattering (GIWAXS).

GIWAXS measurements were performed at SAXS/WAXS beamline, Australian Synchrotron ANSTO. Samples were prepared on Si substrates using identical blend solutions as those used in devices. The 15.2 keV X-ray beam was incident at a grazing angle of 0.08°-0.12°, selected to maximize the scattering intensity from the samples. The scattered x-rays were detected using a Dectris Pilatus 2M photon counting detector.

Contact angles Measurement.

The contact angles were measured using a JC2000D1 contact angle instrument.

Atomic Force Microscopy-Infrared Spectroscopy (AFM-IR) Measurement.

AFM-IR experiments were carried out using a commercial AFM-IR setup (Bruker nanoIR 3) that consists of an AFM microscope operating in contact mode and a Quantum Cascade Laser (QCL laser). The repetition rate of the QCL laser is tunable to match the contact resonance frequencies of the AFM cantilever. In the instrument, a pulsed tunable QCL laser is focused onto a PtIr coated AFM probe via a parabolic mirror, while the microscope is operated in the intermittent contact mode. The readout of the optically induced changes in the sample is performed by providing bimodal excitation of the cantilever and monitoring the response at the second cantilever Eigen-mode, while the first Eigen-mode is used for AFM topography and feedback. The corresponding blend films AFM-IR images were measured at a wavenumber of 2216 cm^{-1}, which is a characteristic absorption peak of SMAs compared with PM6. The film samples were prepared under the same conditions as those used for device fabrication.

Supporting Figures and Tables

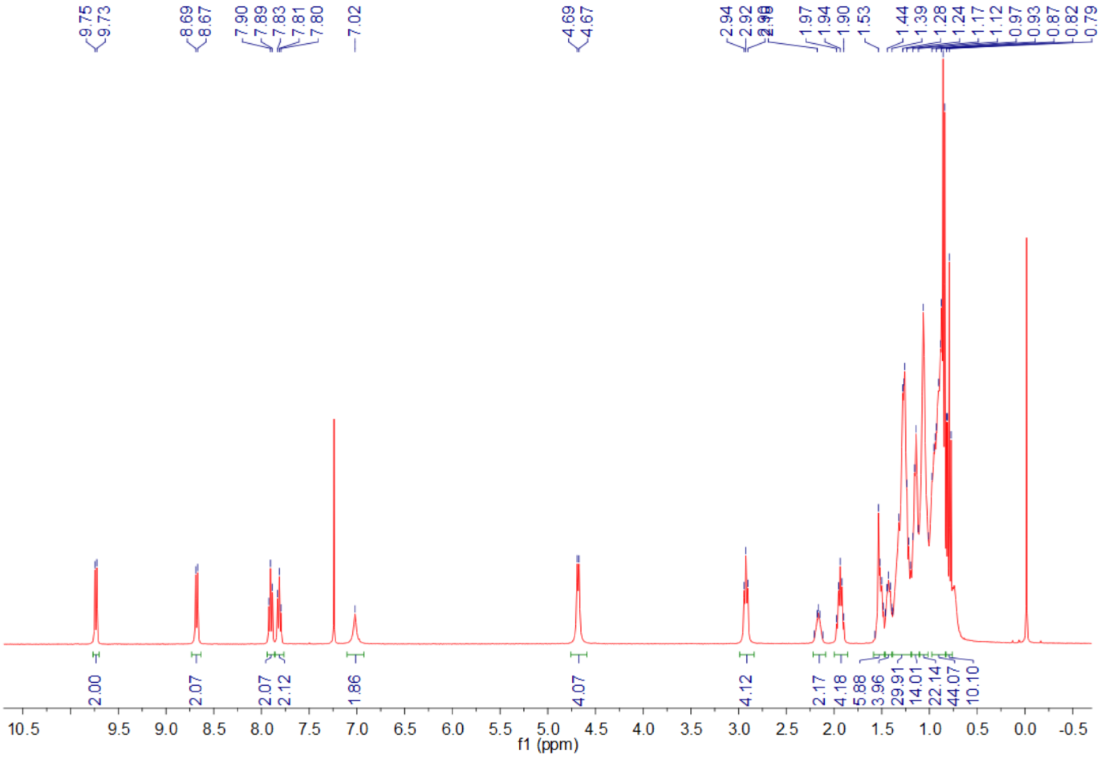

Figure S1. ^{1}H NMR spectra of compound 2 in CDCl$_3$.

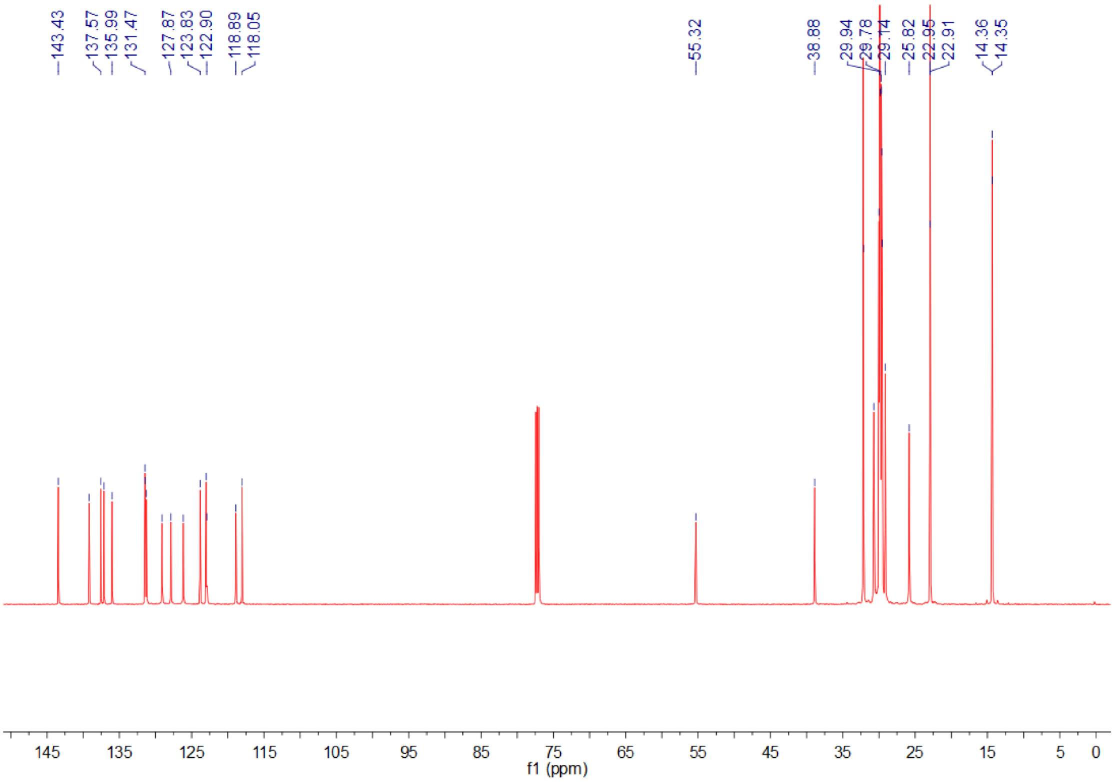

Figure S2. ^{13}C NMR spectra of compound 2 in CDCl$_3$.

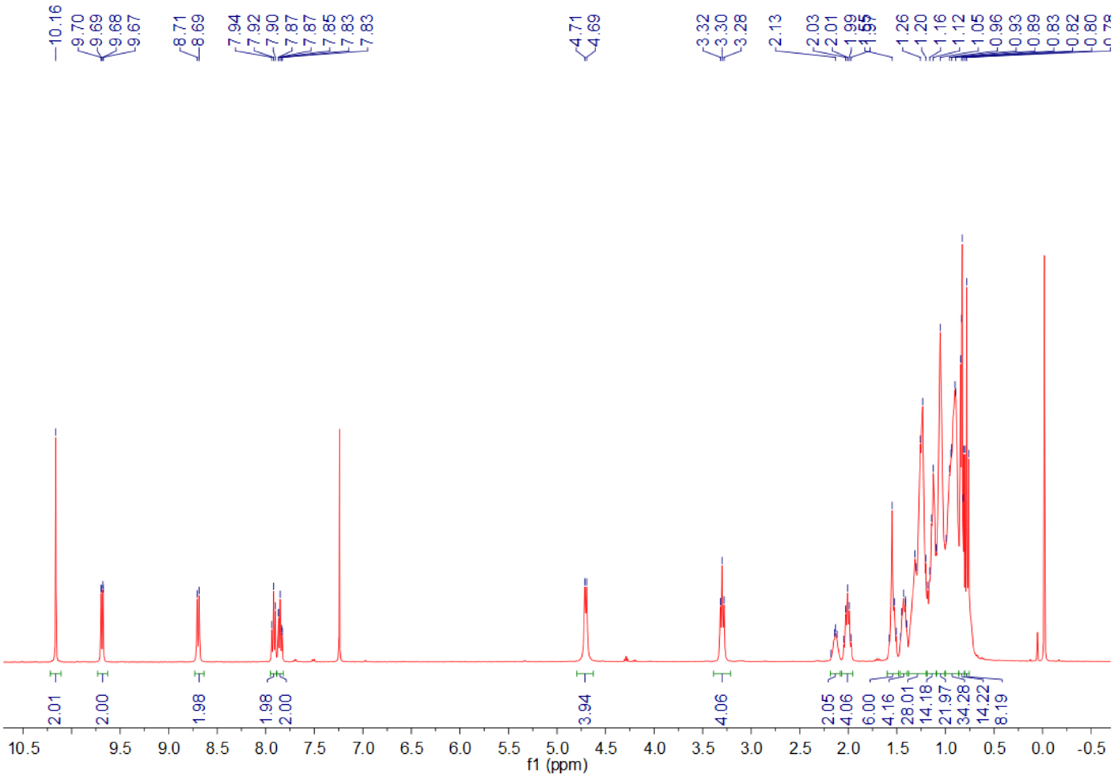

Figure S3. ^{1}H NMR spectra of compound 3 in $CDCl_3$.

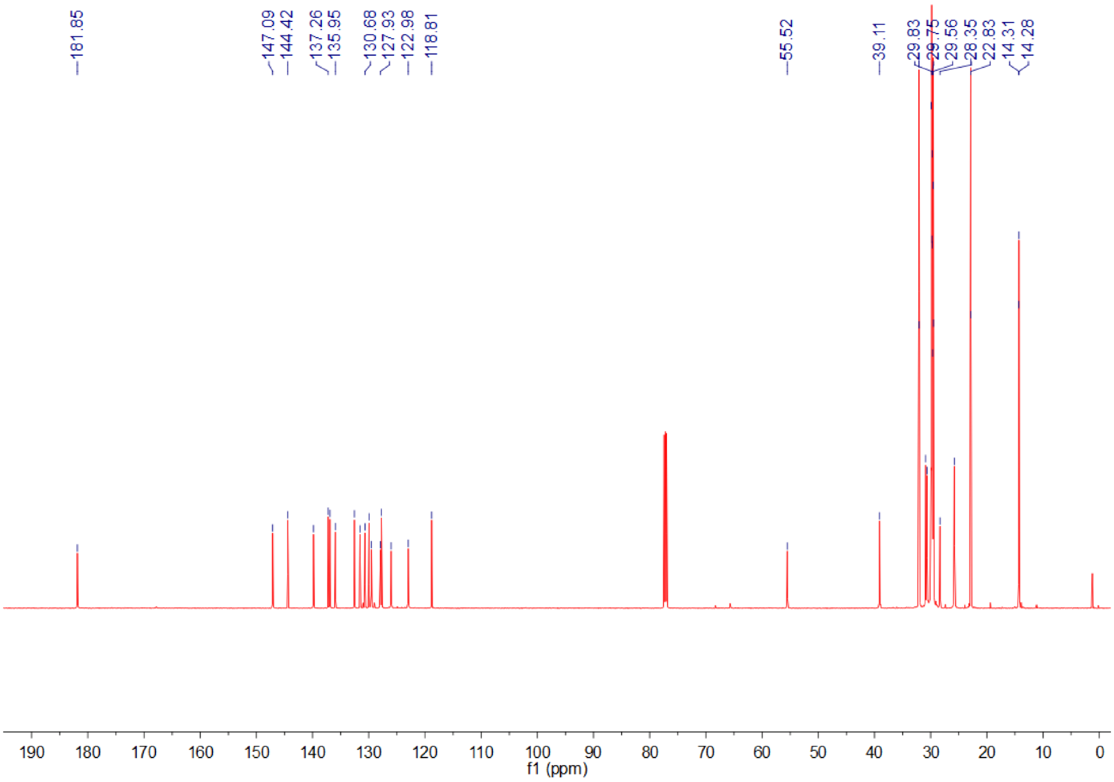

Figure S4. ^{13}C NMR spectra of compound 3 in $CDCl_3$.

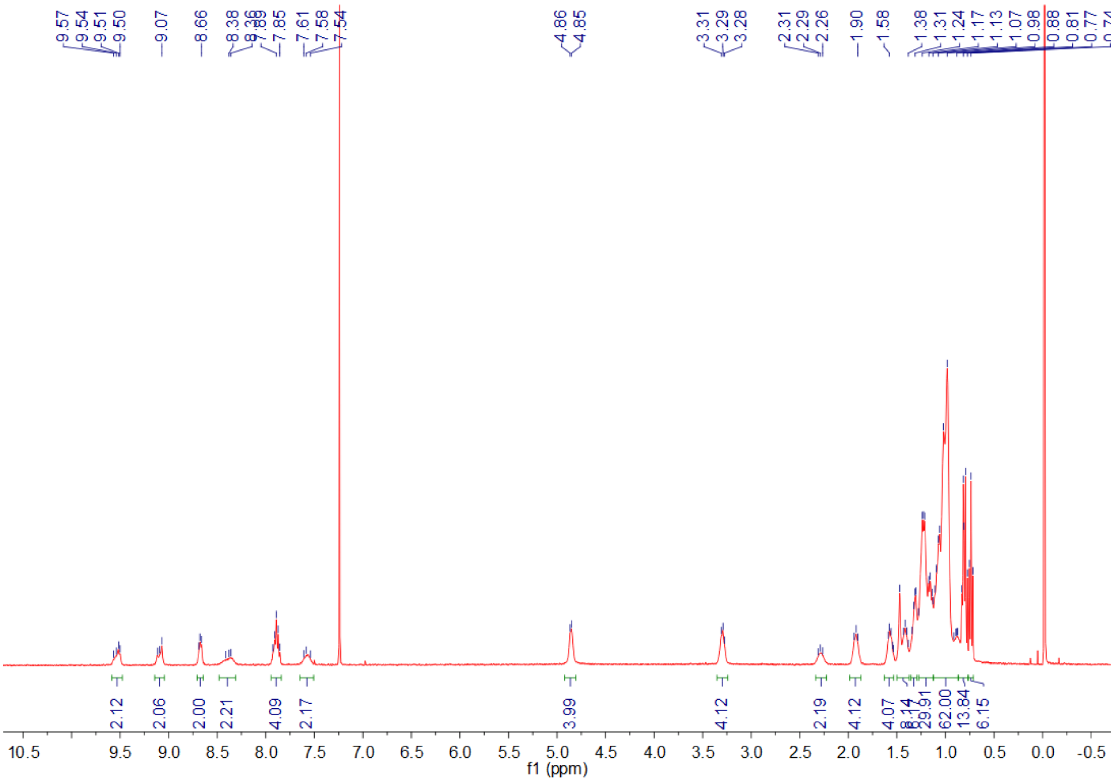

Figure S5. ^{1}H NMR spectra of CH-PHE in CDCl$_3$.

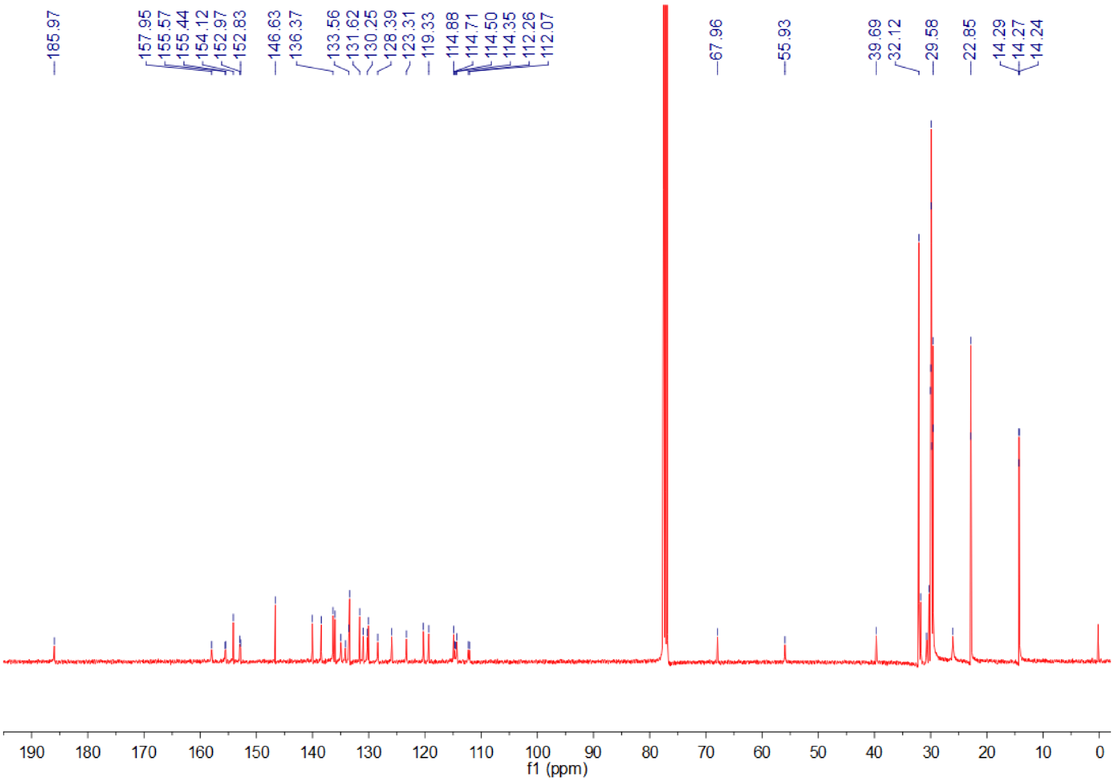

Figure S6. ^{13}C NMR spectra of CH-PHE in CDCl$_3$.

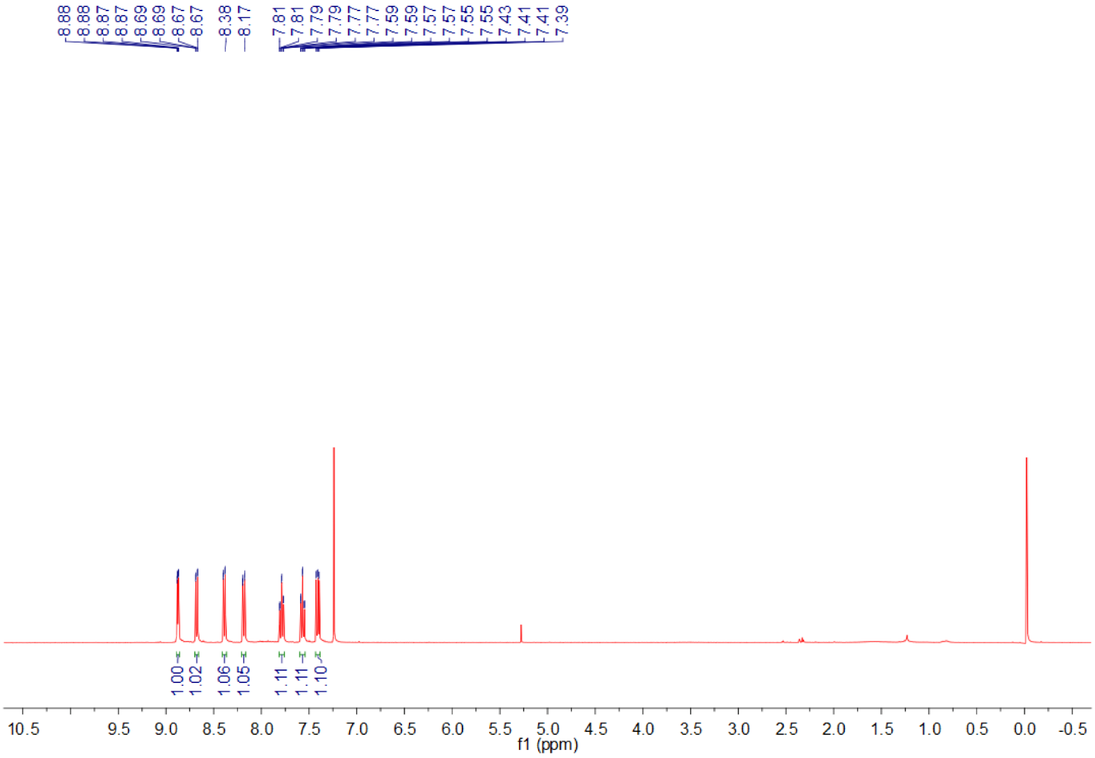

Figure S7. ^{1}H NMR spectra of compound 5 in $CDCl_3$.

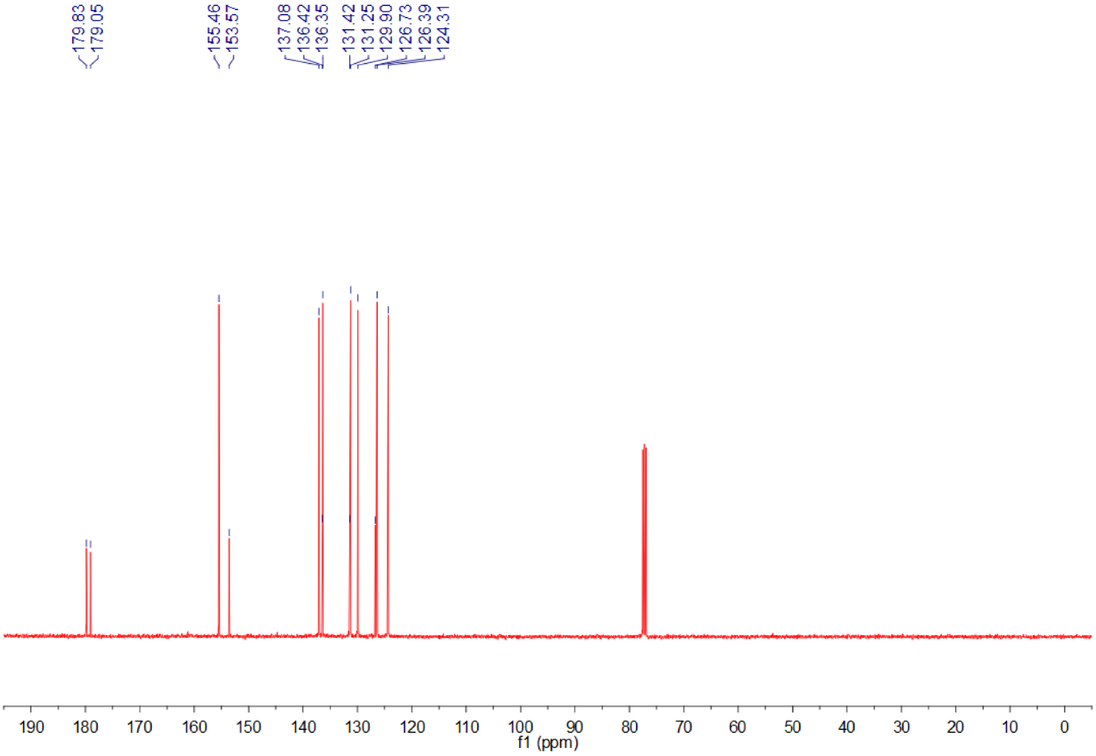

Figure S8. ^{13}C NMR spectra of compound 5 in $CDCl_3$.

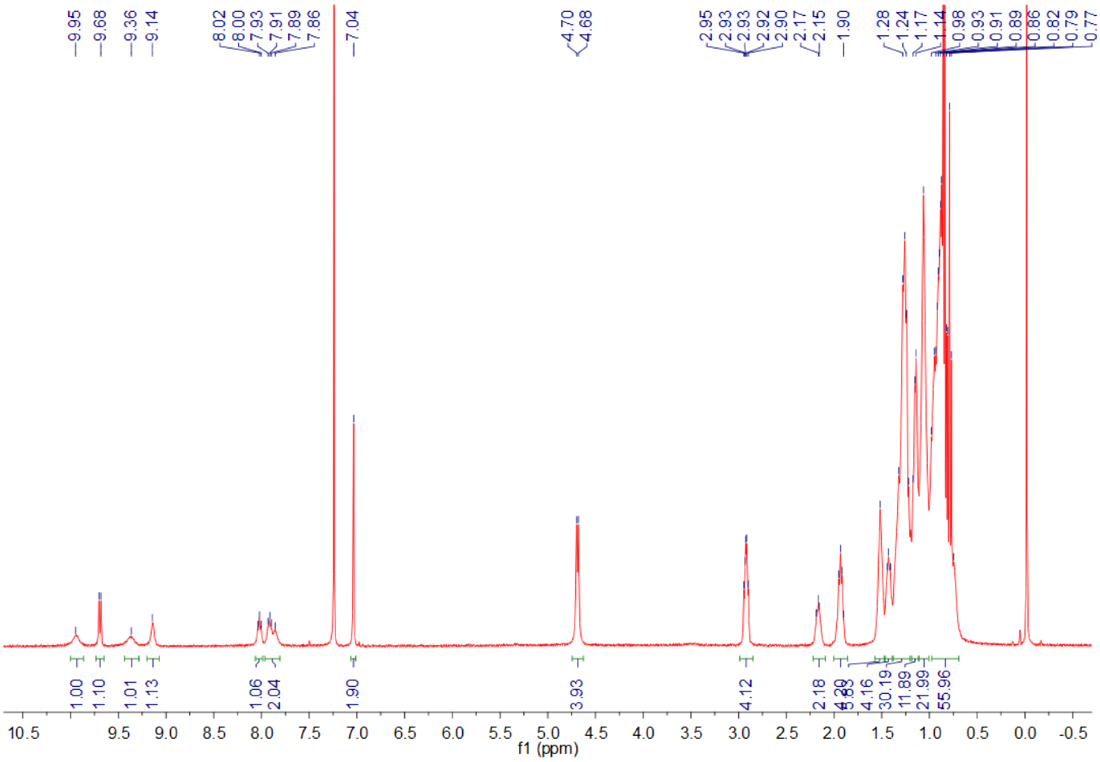

Figure S9. ^{1}H NMR spectra of compound 6 in $CDCl_3$.

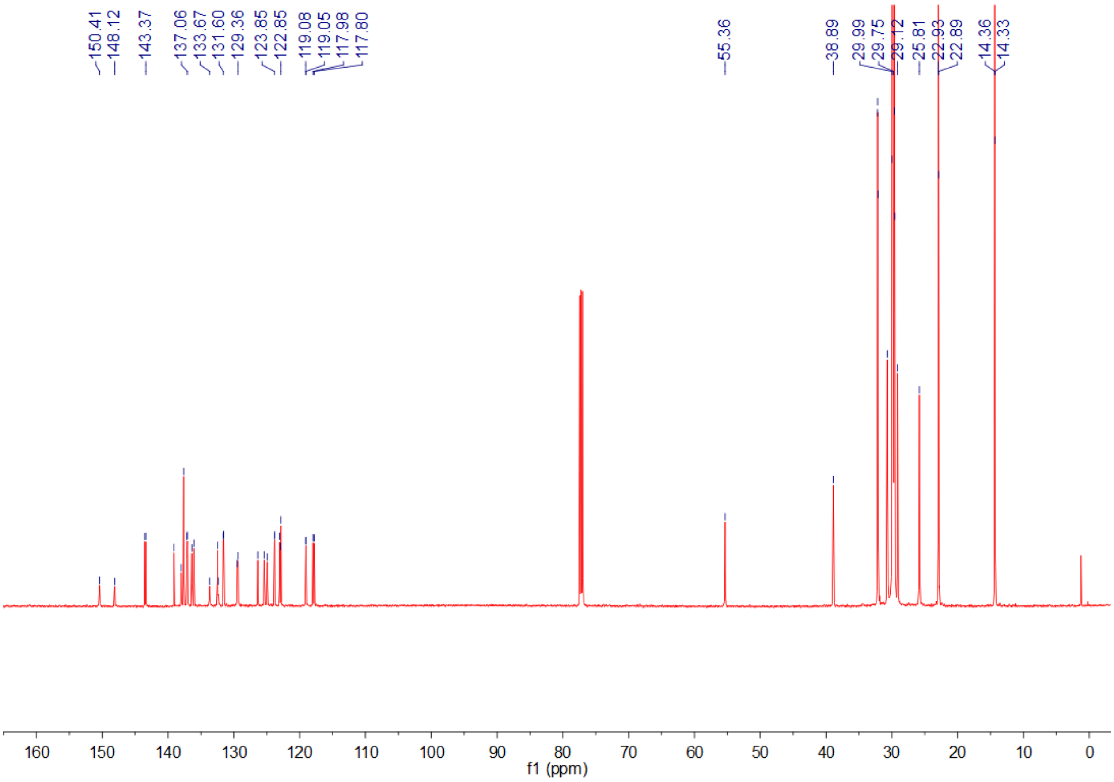

Figure S10. ^{13}C NMR spectra of compound 6 in $CDCl_3$.

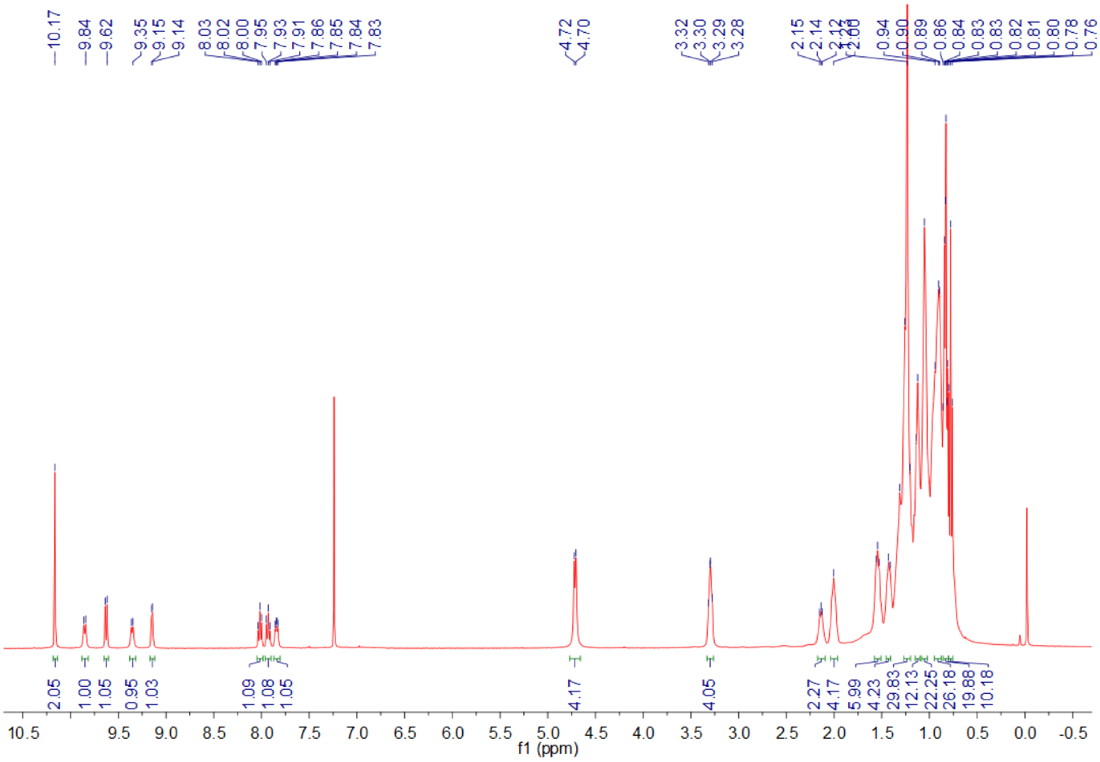

Figure S11. ^{1}H NMR spectra of compound 7 in $CDCl_3$.

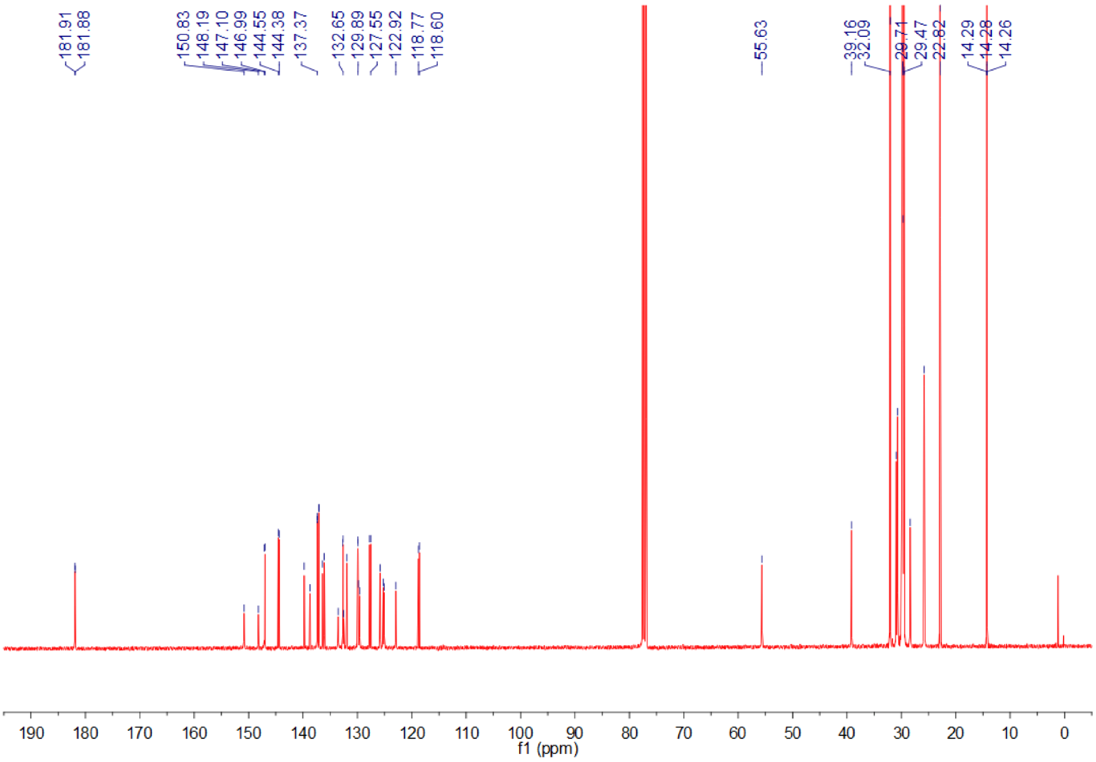

Figure S12. ^{13}C NMR spectra of compound 7 in $CDCl_3$.

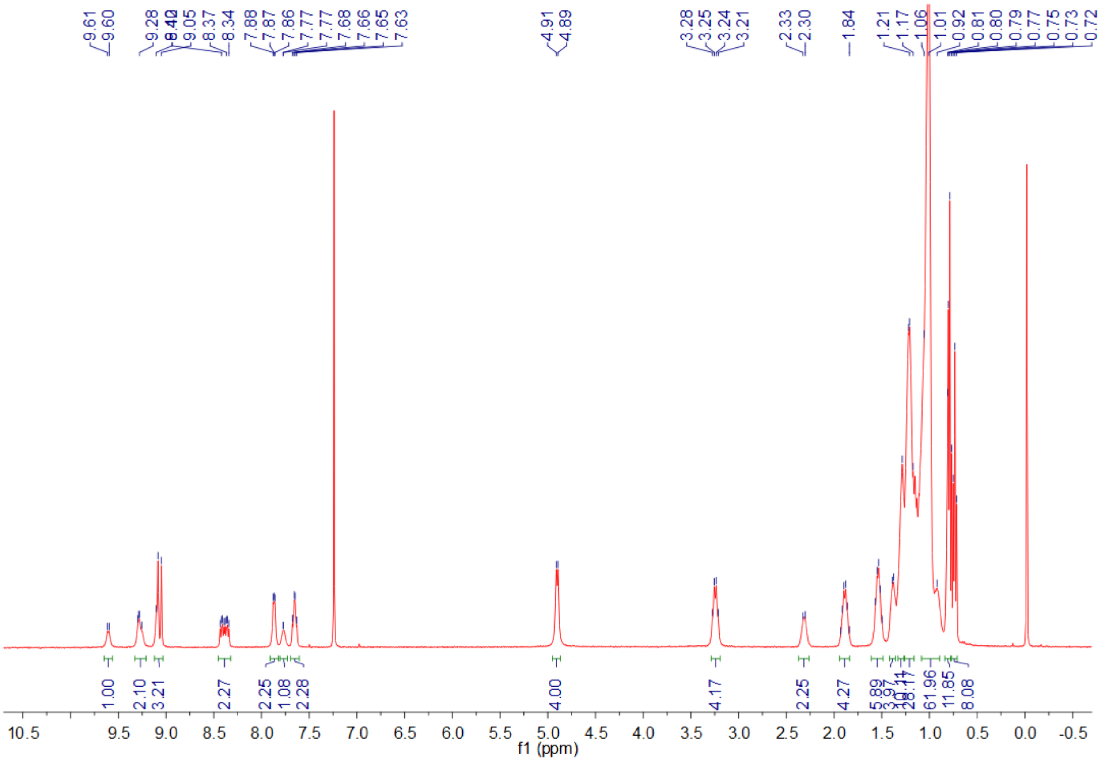

Figure S13. ^{1}H NMR spectra of CH-Bzq in $CDCl_3$.

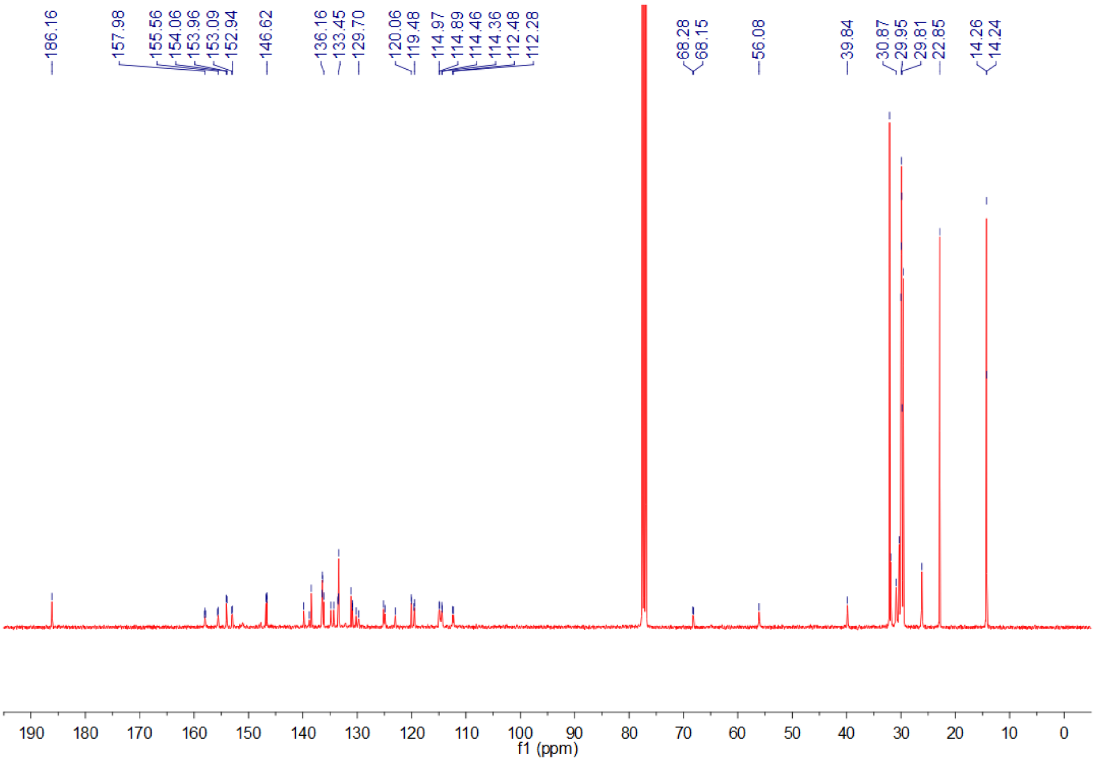

Figure S14. ^{13}C NMR spectra of CH-Bzq in $CDCl_3$.

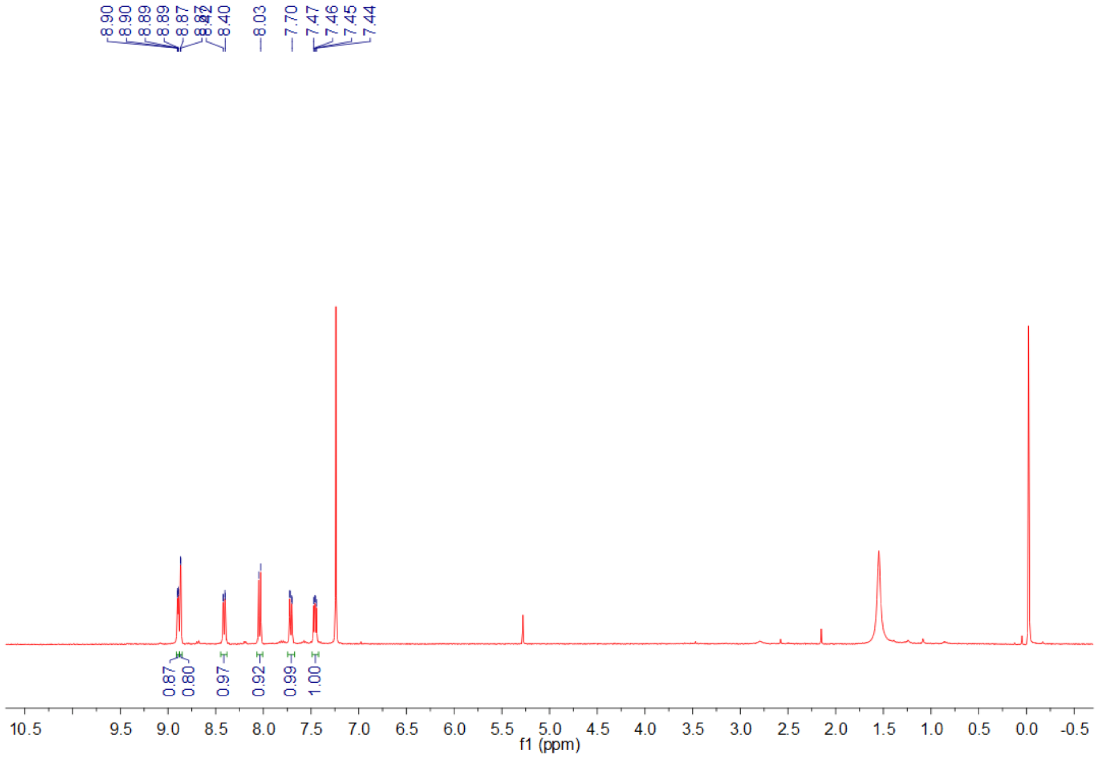

Figure S15. ^{1}H NMR spectra of compound 8 in $CDCl_3$.

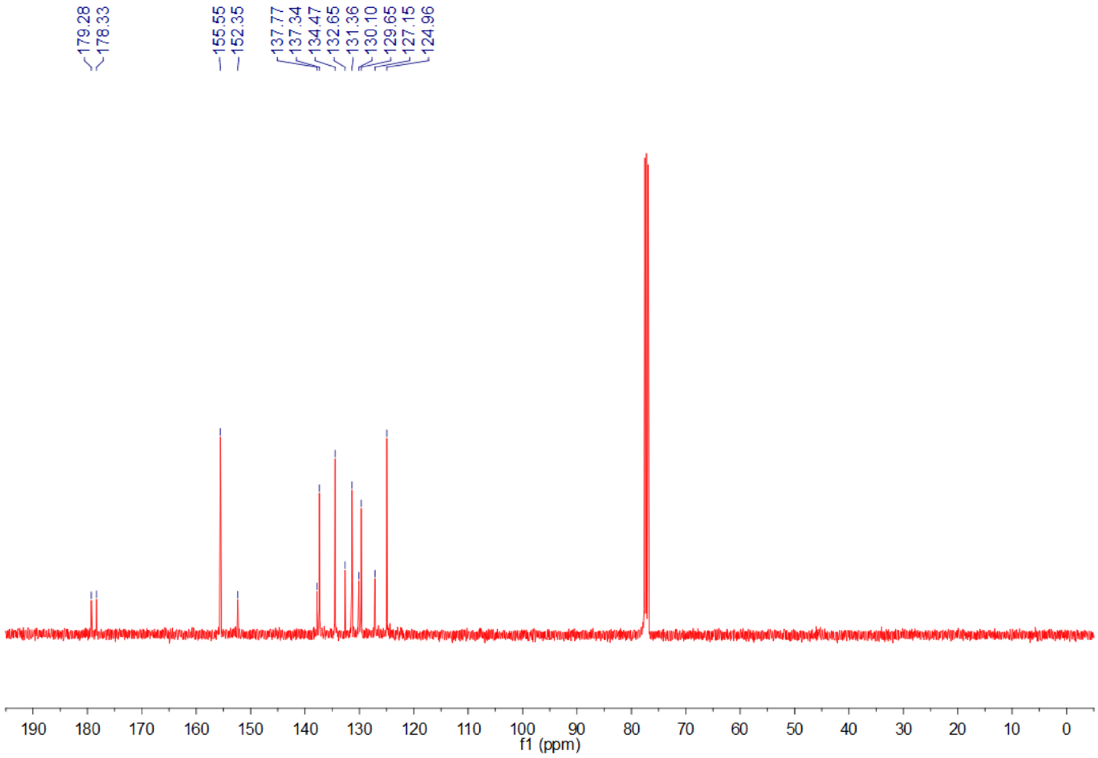

Figure S16. ^{13}C NMR spectra of compound 8 in $CDCl_3$.

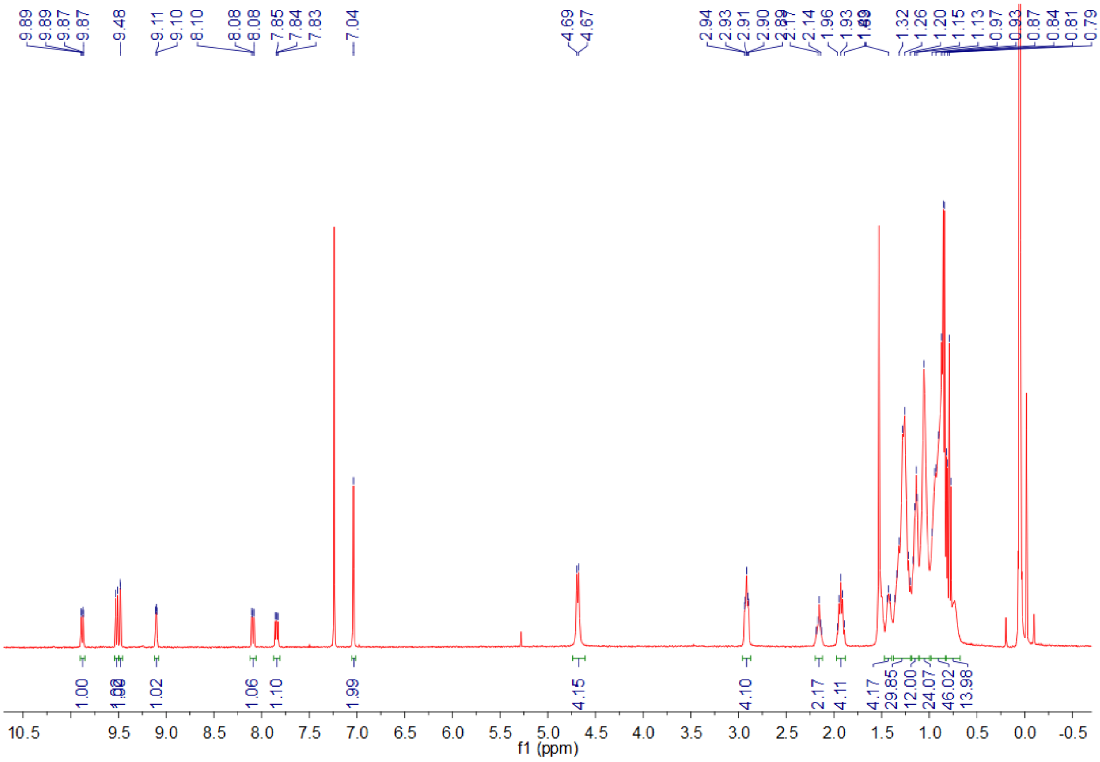

Figure S17. ^{1}H NMR spectra of compound 9 in $CDCl_3$.

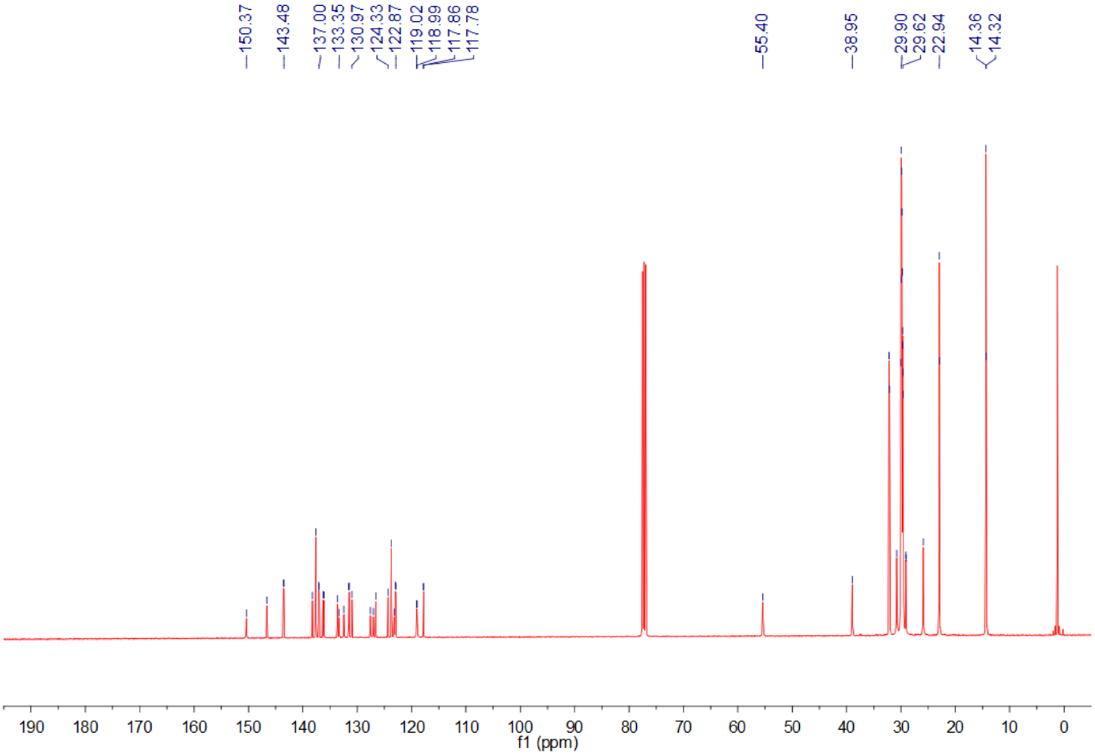

Figure S18. ^{13}C NMR spectra of compound 9 in $CDCl_3$.

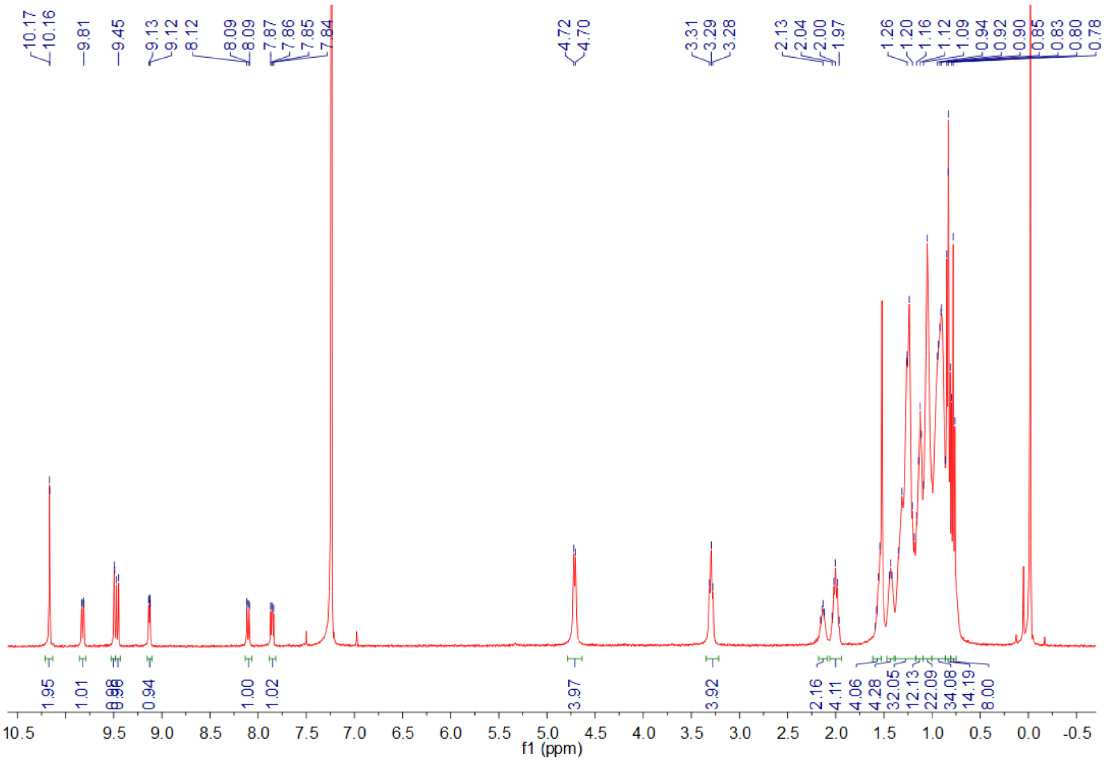

Figure S19. ^{1}H NMR spectra of compound 10 in $CDCl_3$.

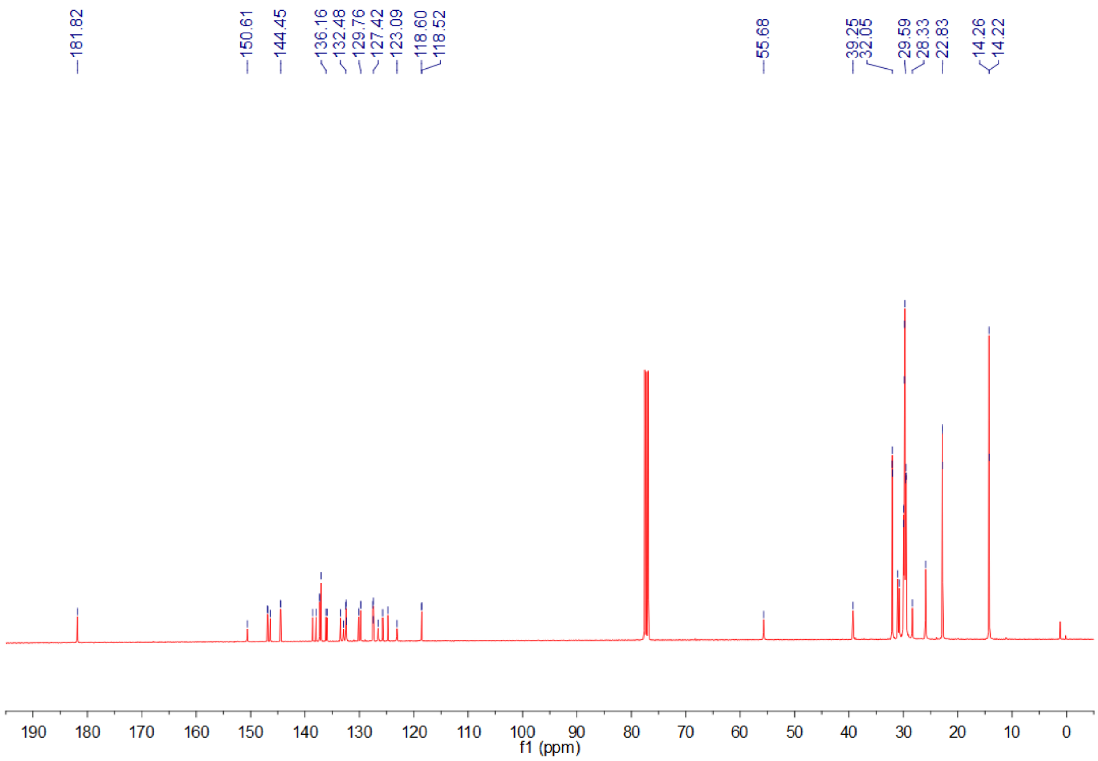

Figure S20. ^{13}C NMR spectra of compound 10 in $CDCl_3$.

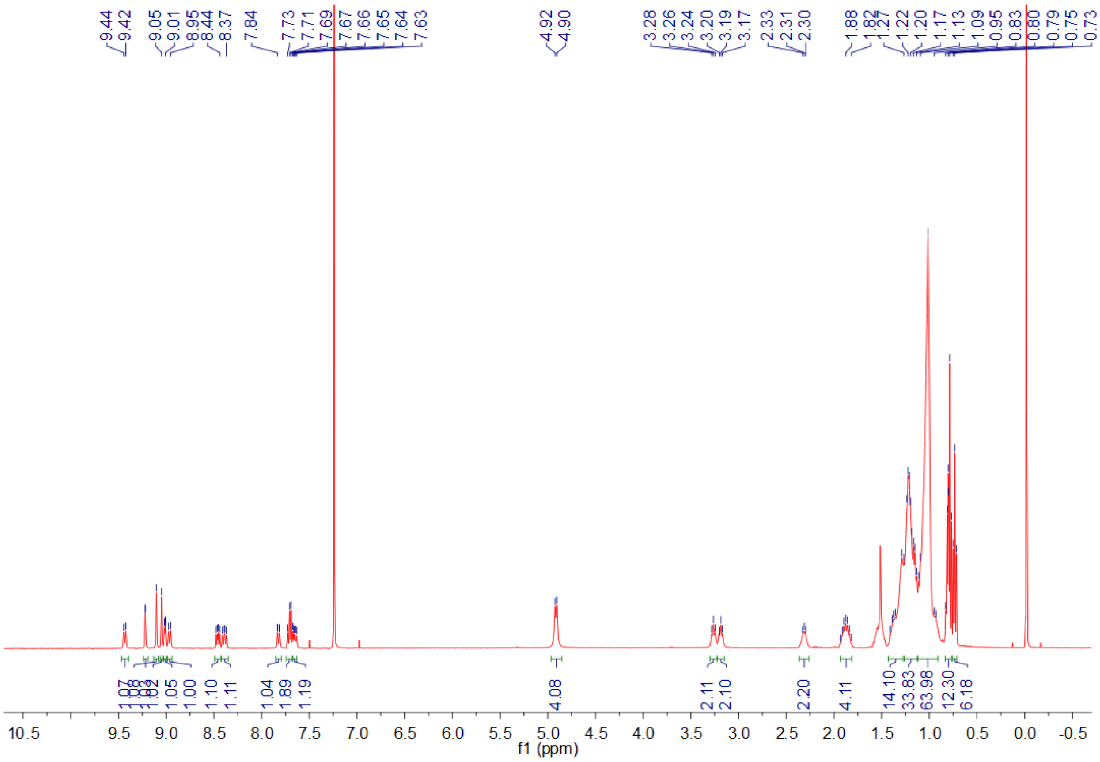

Figure S21. ^{1}H NMR spectra of CH-Bzq-Br in CDCl$_3$.

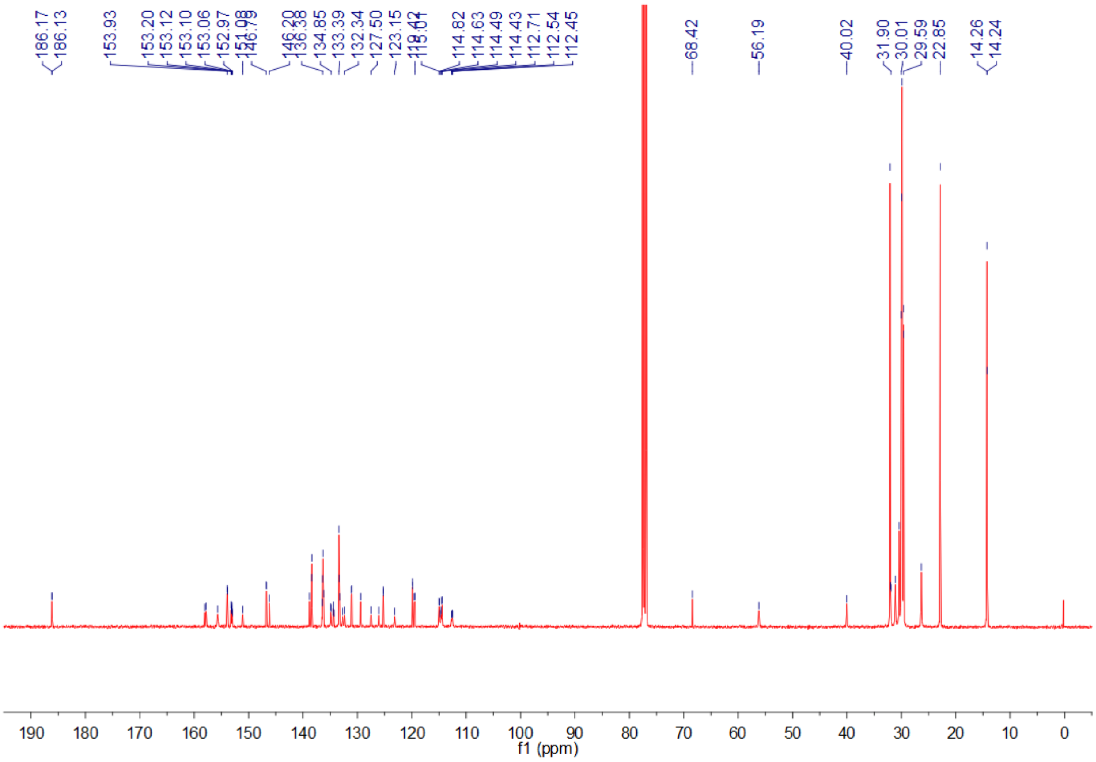

Figure S22. ^{13}C NMR spectra of CH-Bzq-Br in CDCl$_3$.

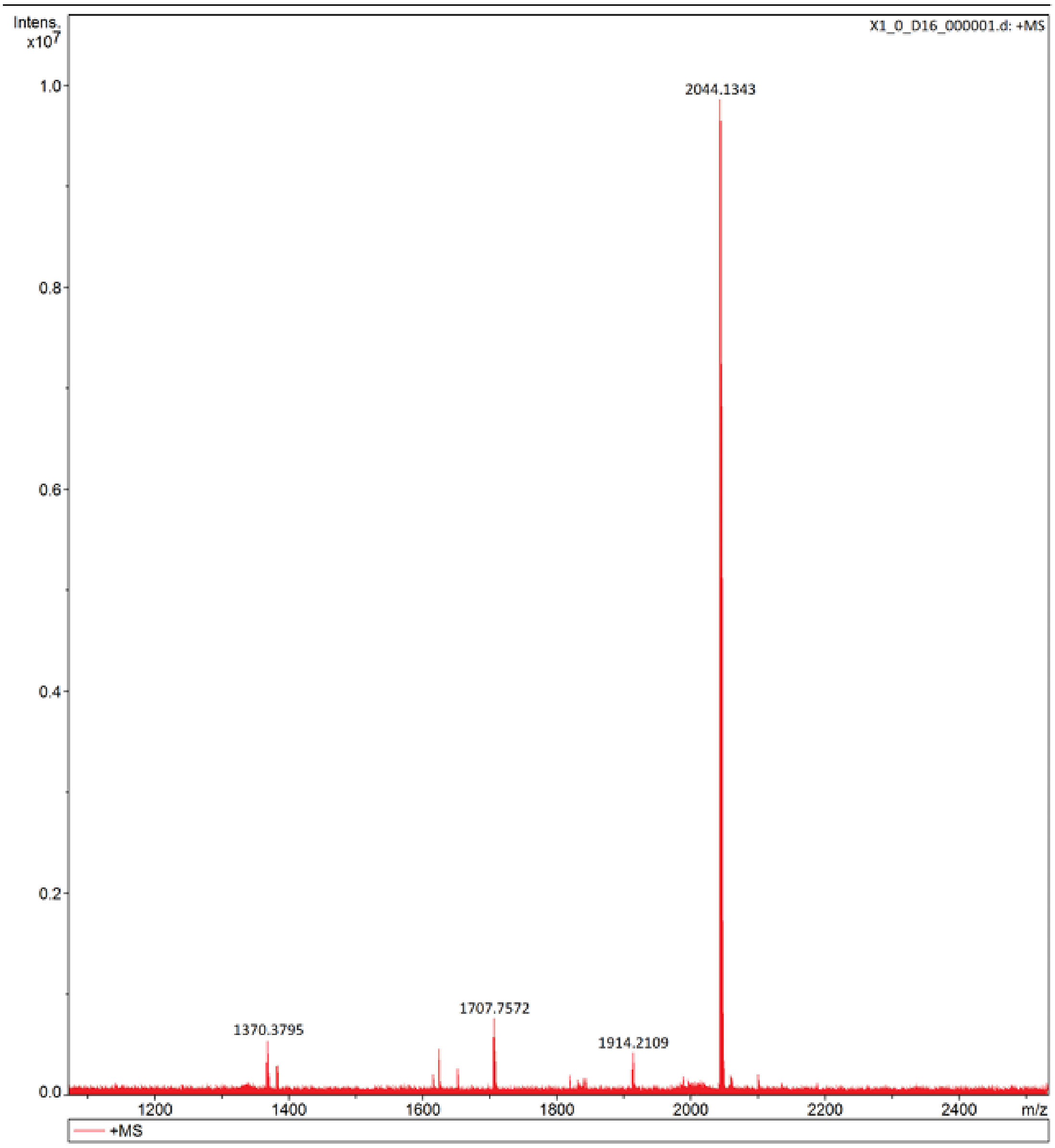

Figure S23. High resolution mass spectrometry (HRMS) of CH-PHE.

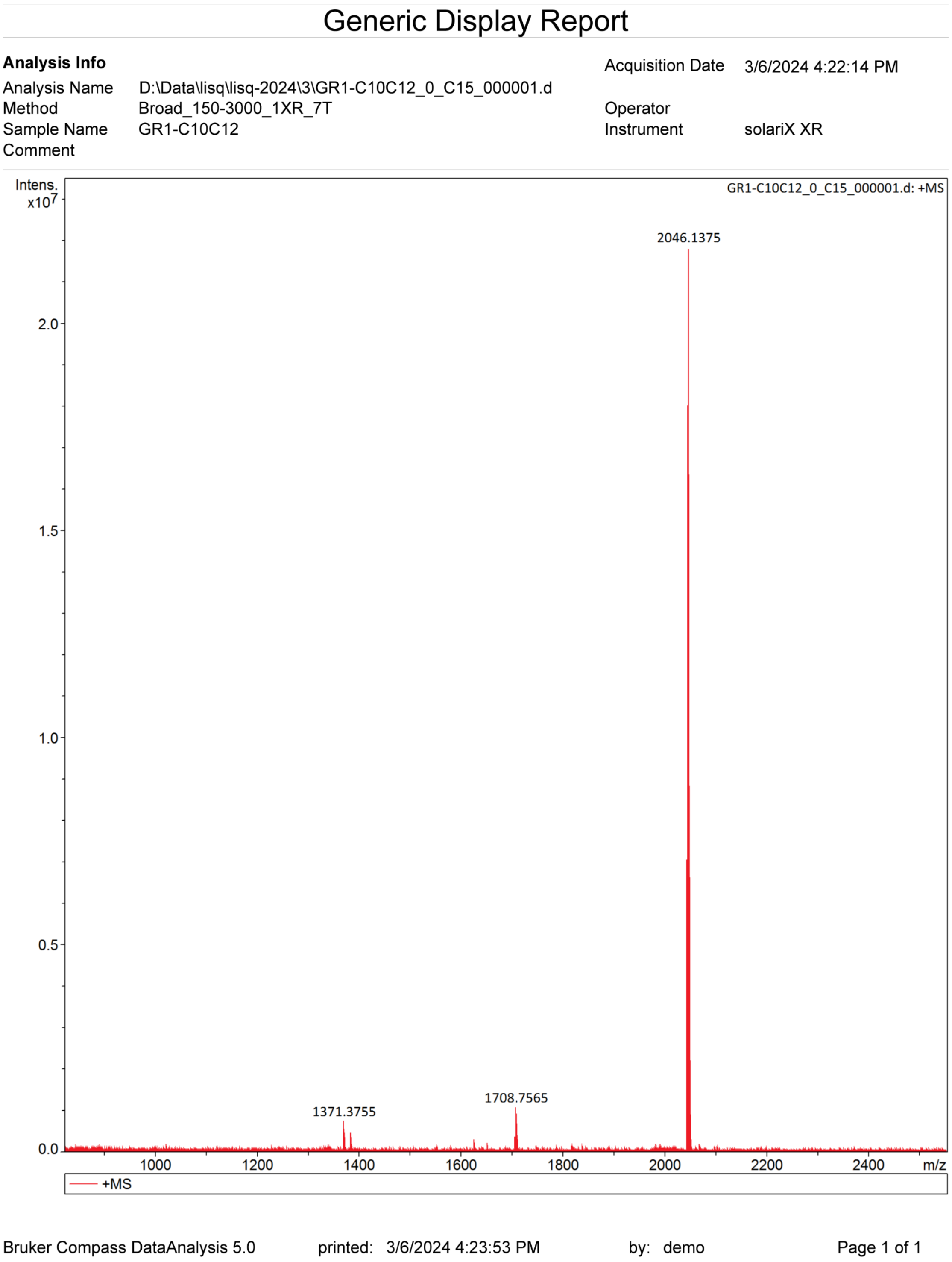

Generic Display Report

Analysis Info

Analysis Name	D:\Data\lisq\lisq-2024\3\GR1-C10C12_0_C15_000001.d	Acquisition Date	3/6/2024 4:22:14 PM
Method	Broad_150-3000_1XR_7T	Operator	
Sample Name	GR1-C10C12	Instrument	solariX XR
Comment			

Bruker Compass DataAnalysis 5.0 printed: 3/6/2024 4:23:53 PM by: demo Page 1 of 1

Figure S24. High resolution mass spectrometry (HRMS) of CH-Bzq.

Generic Display Report

Analysis Info

		Acquisition Date	3/24/2024 7:23:14 PM
Analysis Name	D:\Data\lisq\lisq-2024\3\bzq-9-Br-2tong_000001.d		
Method	Broad_150-3000_1XR_7T	Operator	
Sample Name	bzq-9-Br-2tong	Instrument	solariX XR
Comment			

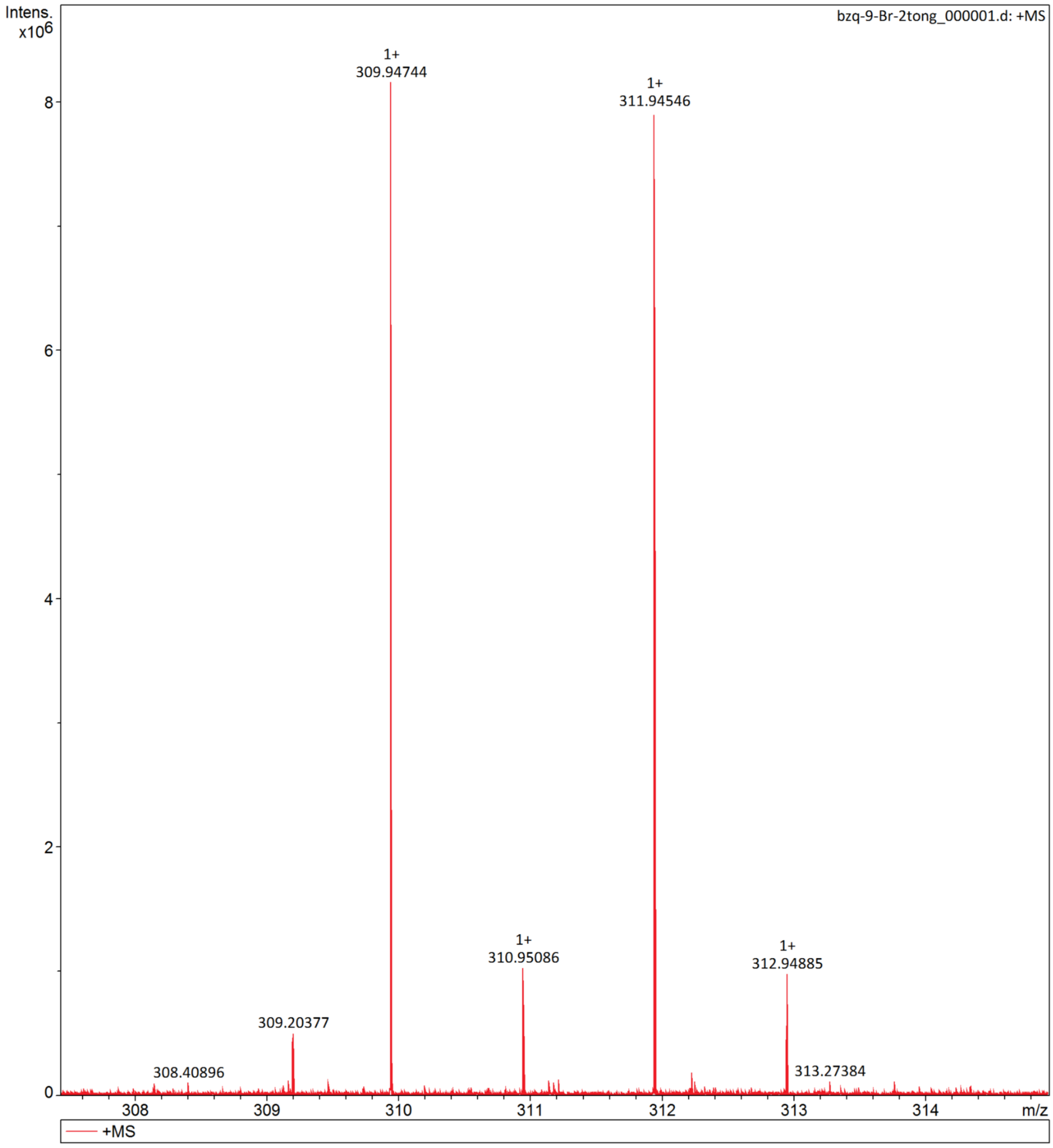

Bruker Compass DataAnalysis 5.0 printed: 3/24/2024 8:21:58 PM by: demo Page 1 of 1

Figure S25. High resolution mass spectrometry (HRMS) of compound 8.

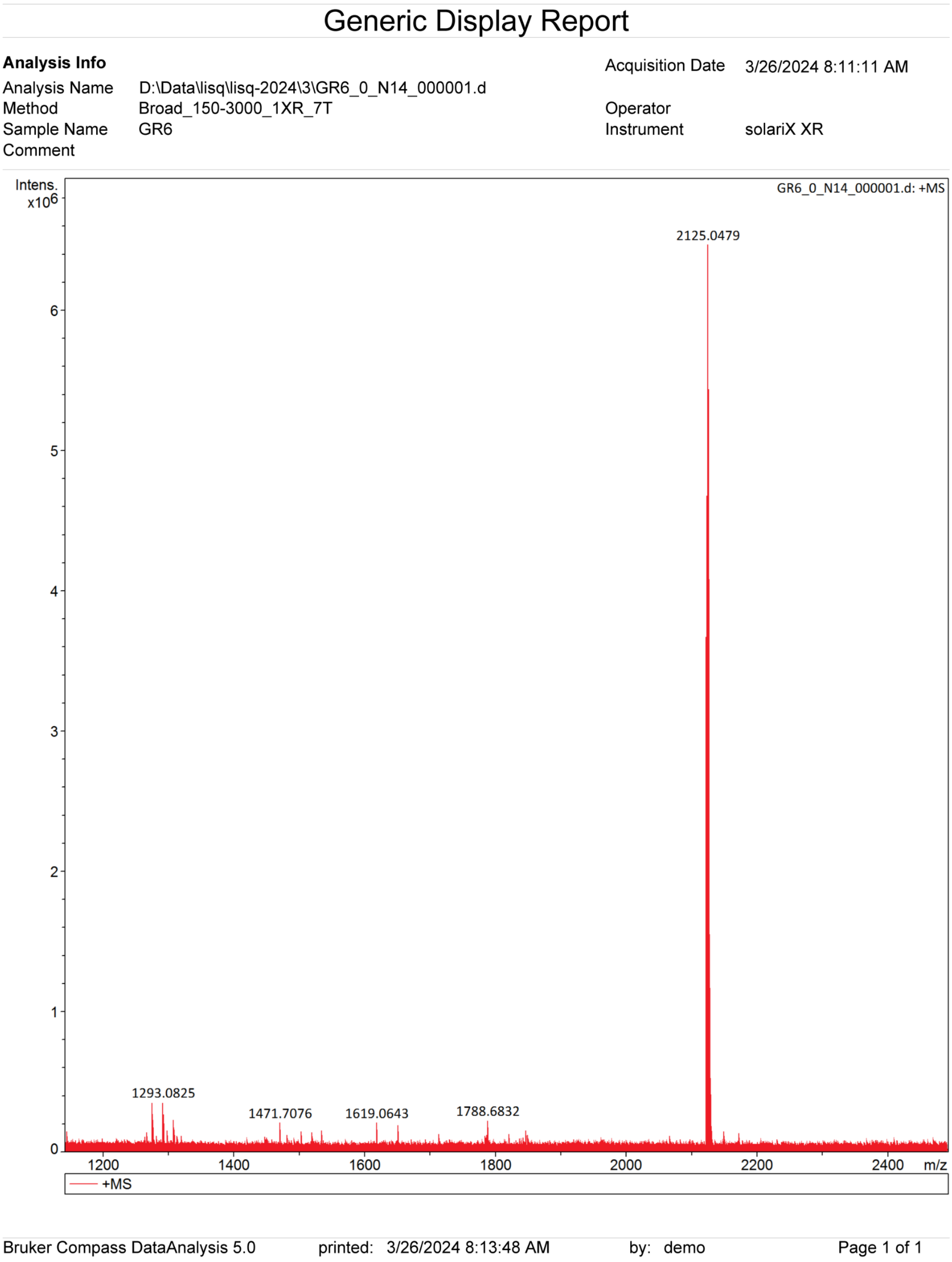

Generic Display Report

Analysis Info

Analysis Name D:\Data\lisq\lisq-2024\3\GR6_0_N14_000001.d
Method Broad_150-3000_1XR_7T
Sample Name GR6
Comment

Acquisition Date 3/26/2024 8:11:11 AM

Operator
Instrument solariX XR

Bruker Compass DataAnalysis 5.0 printed: 3/26/2024 8:13:48 AM by: demo Page 1 of 1

Figure S26. High resolution mass spectrometry (HRMS) of CH-Bzq-Br.

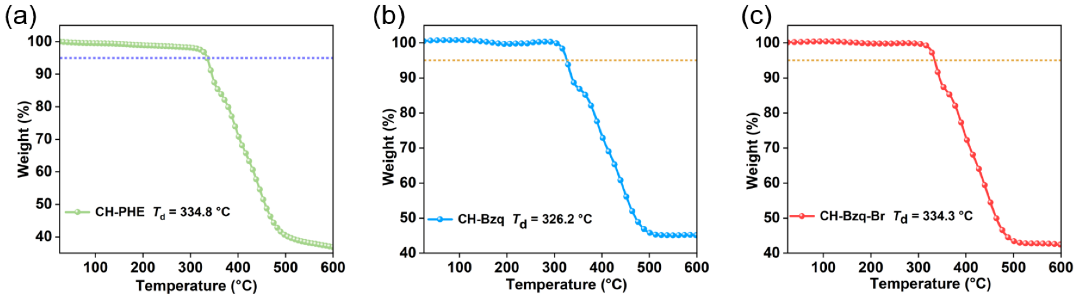

Figure S27. Thermogravimetric analysis (TGA) curves of (a) CH-PHE, (b) CH-Bzq and (c) CH-Bzq-Br.

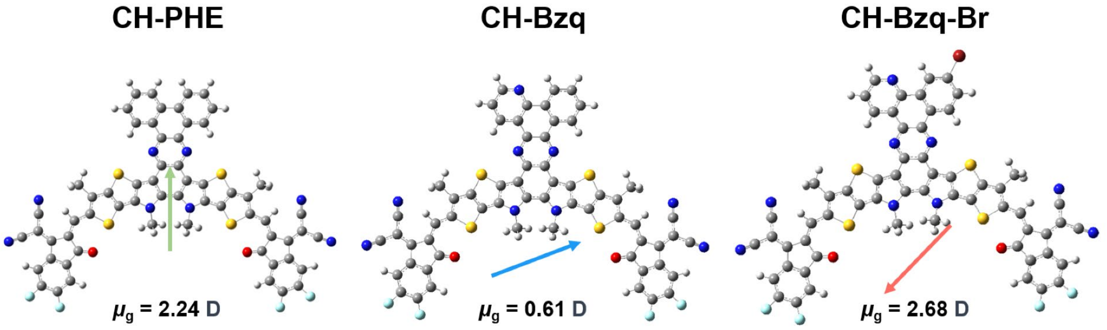

Figure S28. DFT-calculated ground-state dipole moment (μ_g) of CH-PHE, CH-Bzq and CH-Bzq-Br. The arrows represent the ground-state dipole moment direction.

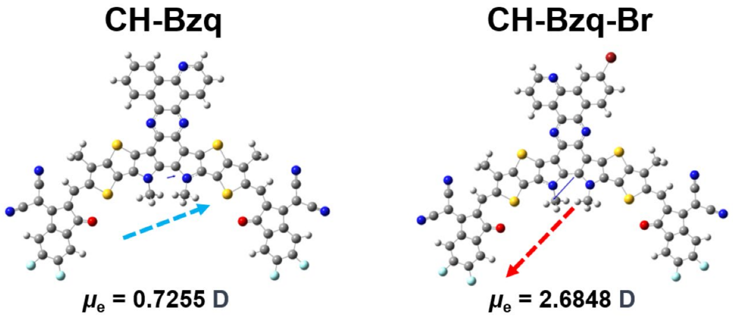

Figure S29. TD-DFT-calculated excited-state dipole moment (μ_e) of CH-Bzq and CH-Bzq-Br. The arrows represent the excited-state dipole moment direction.

Table S1. Theoretical calculated dipole moments of CH-Bzq and CH-Bzq-Br. μ_g = ground state dipole moment, μ_e = excited state dipole moment, $\Delta\mu_{ge}$ = difference between the ground and excited state dipole moments.

Acceptors	μ_g (D)	μ_e (D)	$\Delta\mu_{ge}$ (D)
CH-Bzq	0.61	0.73	0.13
CH-Bzq-Br	2.68	2.68	0.18

Table S2. The detailed values of molecular ground-state dipole moment in x, y and z direction.

Acceptors	μ_g	μ_{gx}	μ_{gy}	μ_{gz}
CH-Bzq	0.61	0.59	0.12	-0.08
CH-Bzq-Br	2.68	-1.93	-1.84	0.24

Table S3. The detailed values of molecular excited-state dipole moment in x, y and z direction.

Acceptors	μ_e	μ_{ex}	μ_{ey}	μ_{ez}
CH-Bzq	0.73	0.69	0.17	-0.14
CH-Bzq-Br	2.68	-2.03	-1.72	0.34

Table S4. Crystallographic and π-π interaction parameters of CH-Bzq and CH-Bzq-Br.

Acceptors	Packing modes	Intermolecular potentials (kJ/mol)	$d_{\pi\text{-}\pi}$ (Å)	$d_{\text{S-N}}$ (Å)	$d_{\text{S-O}}$ (Å)
CH-Bzq	Mode 1 (E/E)	-187.3	3.437	3.344/3.346	2.679/2.690
	Mode 2 (Dual E/C-1)	-374.8	3.381		
	Mode 3 (Dual E/C-2)	-342.8	3.403		
CH-Bzq-Br	Mode 1 (E/E)	-148.9	3.447	3.297/3.345	2.686/2.704
	Mode 2 (Dual E/C-1)	-403.3	3.359		
	Mode 3 (Dual E/C-2)	-364.2	3.382		

Table S5. Crystal data and structure refinement for CH-Bzq and CH-Bzq-Br.

Compound	CH-Bzq	CH-Bzq-Br
CCDC number	2375434	2375436
Empirical formula	$C_{126}H_{155}F_4N_9O_2S_4$	$C_{127}H_{156}BrF_4N_9O_2S_4$
Formula weight	2031.82	2124.75
Temperature/K	193.00	193.00
Crystal system	triclinic	triclinic
Space group	P-1	P-1
a/Å	17.182(3)	17.430(5)
b/Å	19.052(4)	18.929(5)
c/Å	19.726(4)	19.665(5)
α/°	104.389(9)	104.767(8)
β/°	108.549(9)	108.463(9)
γ/°	92.542(9)	91.368(8)
Volume/Å^3	5876(2)	5912(3)
Z	2	2
ρ_{calc}g/cm^{-3}	1.148	1.194
μ/mm^{-1}	0.787	1.049
F(000)	2180.0	2264.0
Crystal size/mm^3	0.12 × 0.11 × 0.08	0.12 × 0.11 × 0.08
Radiation	GaKα (λ = 1.34139)	GaKα (λ = 1.34139)
2Θ range for data collection/°	4.278 to 107.814	4.288 to 105.962
Index ranges	$-20 \leq h \leq 20$, $-22 \leq k \leq 22$, $-23 \leq l \leq 23$	$-20 \leq h \leq 20$, $-22 \leq k \leq 22$, $-19 \leq l \leq 23$
Reflections collected	63726	57113
Independent reflections	21015 [R_{int} = 0.0638, R_{sigma} = 0.0771]	20251 [R_{int} = 0.1370, R_{sigma} = 0.1682]
Data/restraints/parameters	21015/534/1308	20251/1169/1312
Goodness-of-fit on F^2	1.084	1.175
Final R indexes [I>=2σ (I)]	R_1 = 0.1323, wR_2 = 0.3177	R_1 = 0.1554, wR_2 = 0.3485
Final R indexes [all data]	R_1 = 0.1953, wR_2 = 0.3508	R_1 = 0.2932, wR_2 = 0.4025
Largest diff. peak/hole/e Å^{-3}	0.55/-0.50	0.64/-0.82

The X-ray diffraction signals of single crystals were collected on Rigaku XtalAB PRO MM007 DW at 193 K.

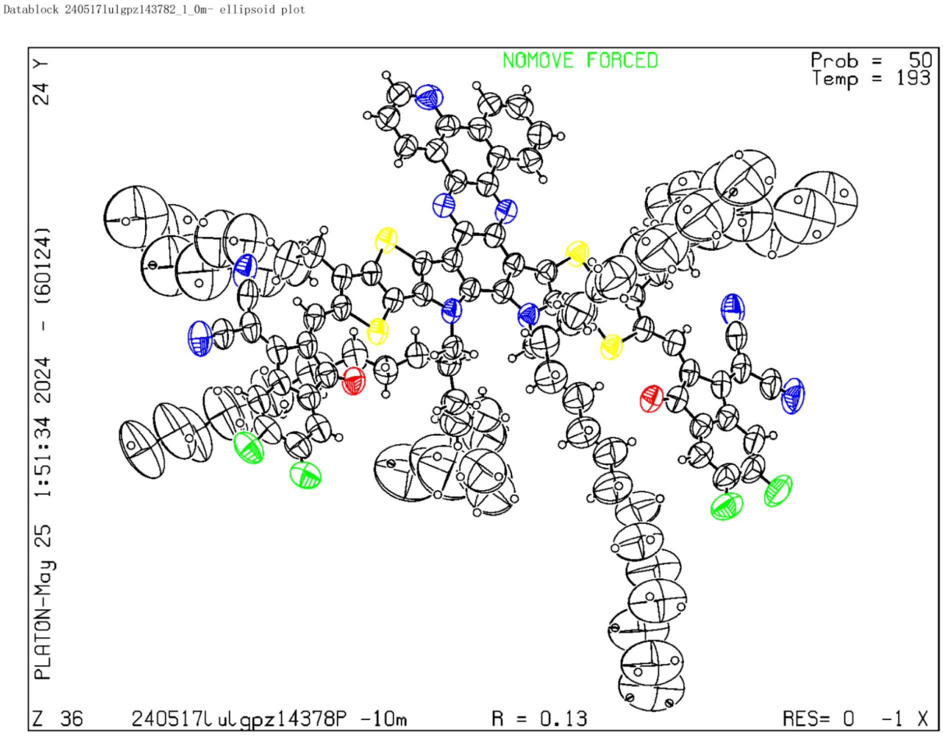

Figure S30. The ORTEP-style illustration with probability ellipsoids of CH-Bzq (CCDC: 2375434).

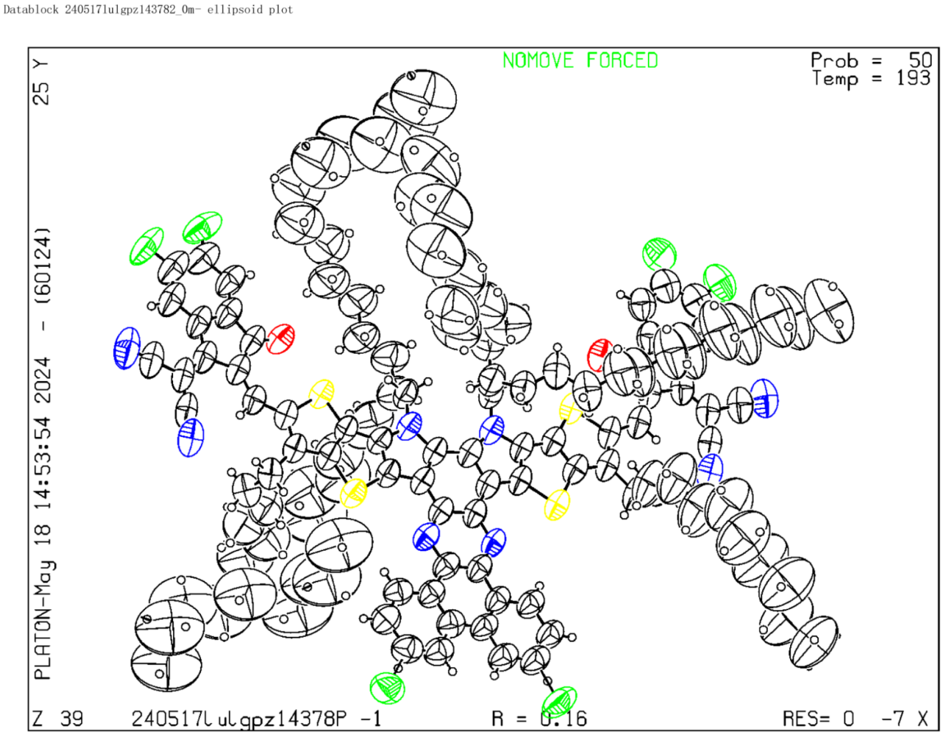

Figure S31. The ORTEP-style illustration with probability ellipsoids of CH-Bzq-Br (CCDC: 2375436).

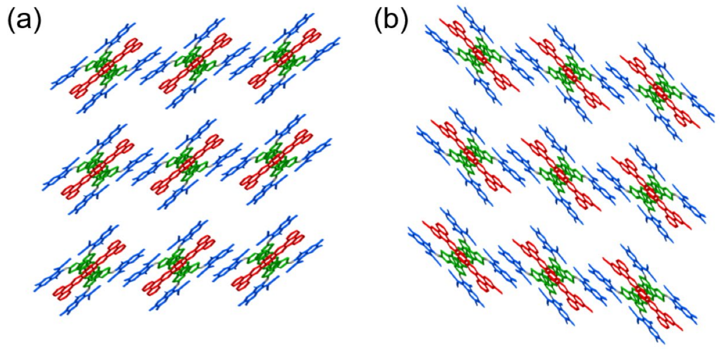

Figure S32. The molecular packing patterns of (a) CH-Bzq and (b) CH-Bzq-Br in the single-crystal structure.

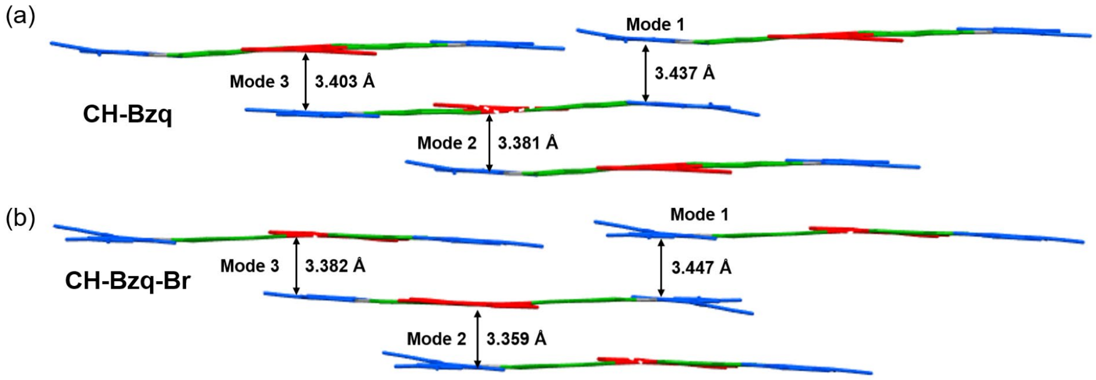

Figure S33. Interlayer π-π stacking distances including all the corresponding intermolecular packing modes of (a) CH-Bzq and (b) CH-Bzq-Br.

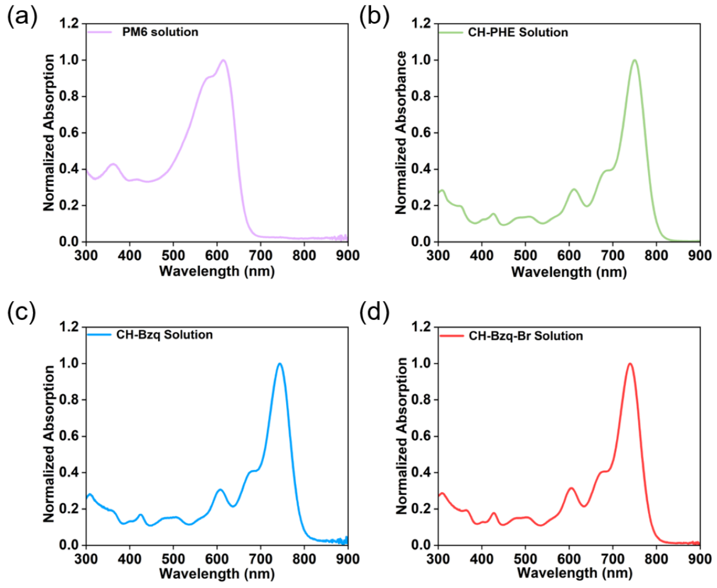

Figure S34. Normalized UV-vis absorption spectra of diluted chloroform solution for (a) PM6, (b) CH-PHE, (c) CH-Bzq and (d) CH-Bzq-Br.

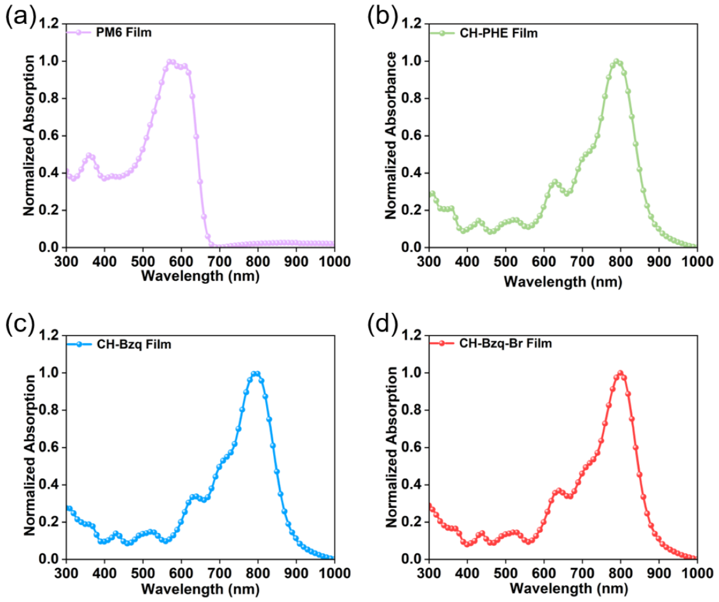

Figure S35. Normalized UV-vis absorption spectra of neat thin films for (a) PM6, (b) CH-PHE, (c) CH-Bzq and (d) CH-Bzq-Br.

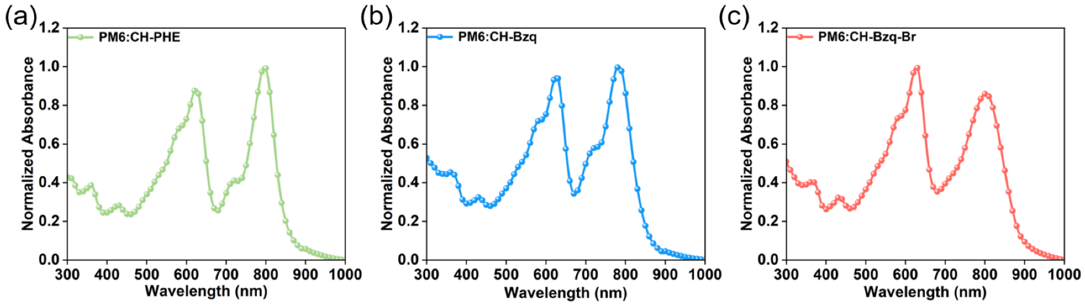

Figure S36. Normalized UV-vis absorption spectra of blend films for (a) PM6:CH-PHE, (b) PM6:CH-Bzq and (c) PM6:CH-Bzq-Br processed from chloroform.

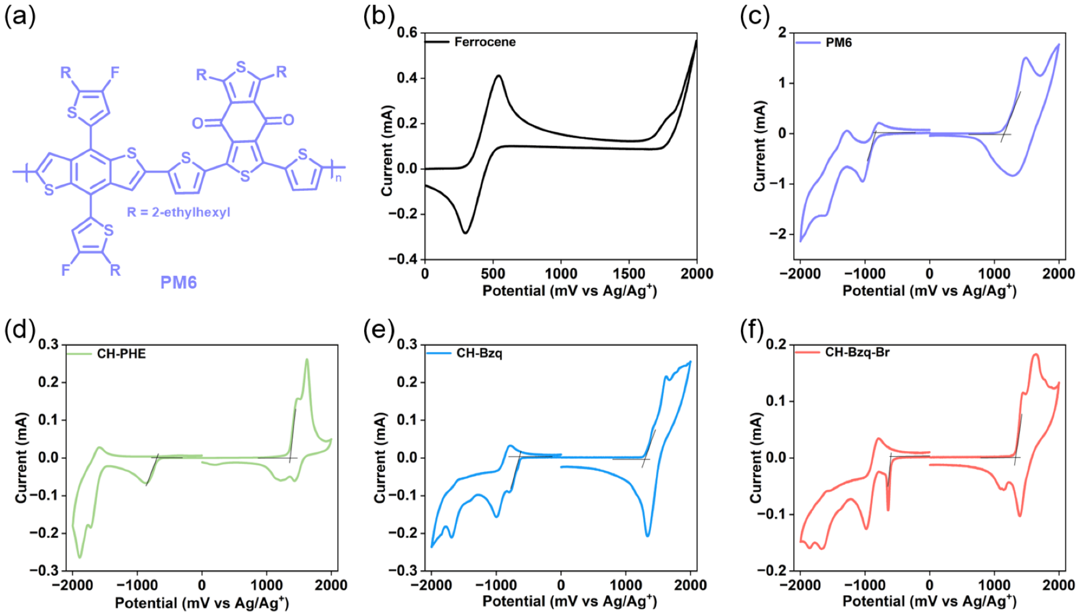

Figure S37. (a) Chemical structure of PM6. Cyclic voltammograms of (b) Ferroence, (c) PM6, (d) CH-PHE, (e) CH-Bzq and (f) CH-Bzq-Br, respectively. PM6, CH-PHE, CH-Bzq, and CH-Bzq-Br solutions were deposited on the surface of working electrode to form their corresponding films, respectively.

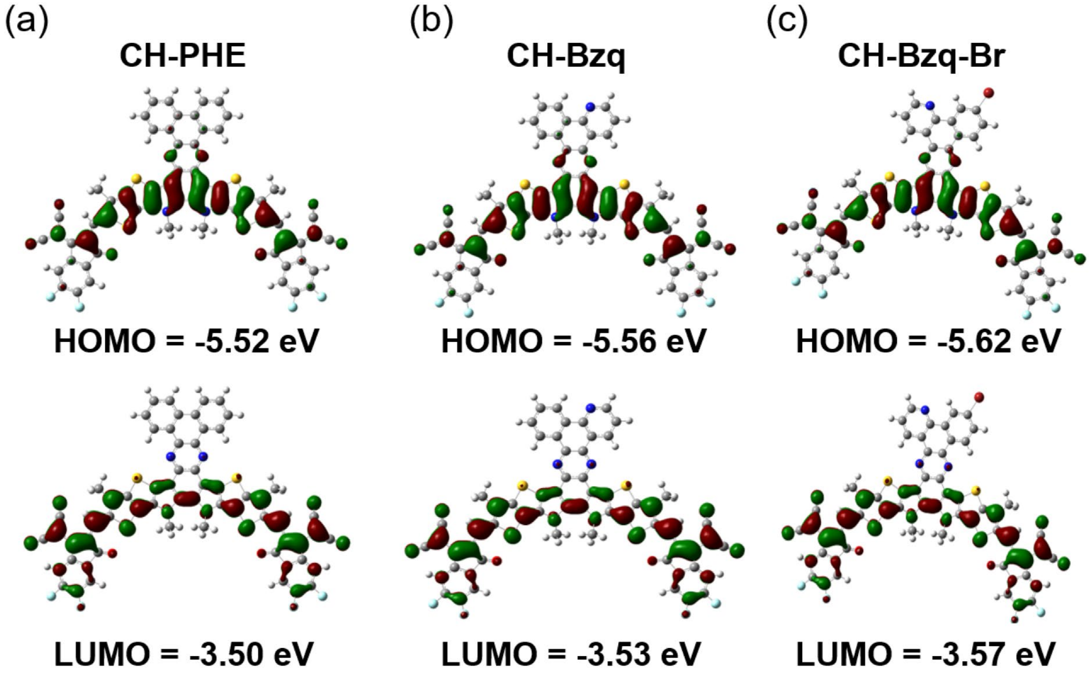

Figure S38. Theoretical density distribution for the frontier molecular orbits of (a) CH-PHE, (b) CH-Bzq and (c) CH-Bzq-Br.

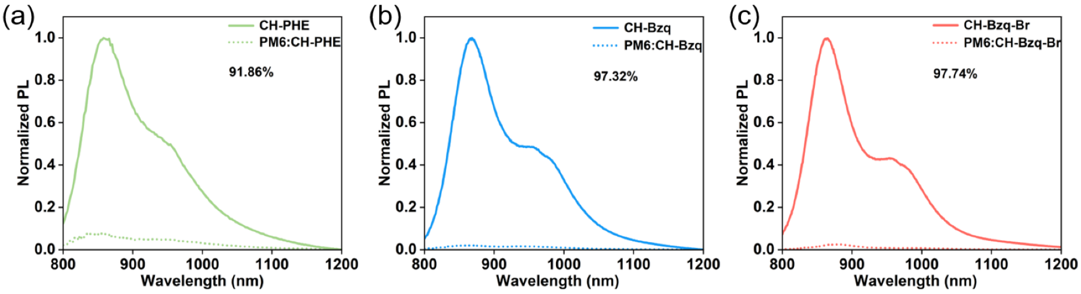

Figure S39. Steady-state photoluminescence (PL) quenching spectra of (a) CH-PHE, (b) CH-Bzq and (c) CH-Bzq-Br-based neat and blend films excited at 760 nm.

Table S6. Detailed photovoltaic parameters of the PM6:CH-Bzq-Br based devices processed by varied D:A ratios under the illumination of AM 1.5G Illumination (100 mW cm^{-2}).

D:A(w/w)	V_{oc} (V)	J_{sc} (mA/cm^2)	FF (%)	PCE (%)
1:1	0.934	25.74	76.09	18.29
1:1.1	0.931	25.92	75.97	18.33
1:1.2	0.930	26.40	76.41	18.76
1:1.3	0.931	26.26	75.54	18.46

Table S7. Detailed photovoltaic parameters of the PM6:CH-Bzq-Br based devices processed by varied addition ratio of TCB under the illumination of AM 1.5G Illumination (100 mW cm^{-2}).

TCB (mg/ml)	V_{oc} (V)	J_{sc} (mA/cm^2)	FF (%)	PCE (%)
5	0.930	26.32	77.08	18.87
8	0.930	26.86	76.35	19.07
10	0.929	27.26	76.22	19.30
12	0.930	26.76	76.80	19.11

Table S8. Detailed photovoltaic parameters of the PM6:CH-Bzq-Br based devices processed by varied thermal annealing temperature under the illumination of AM 1.5G Illumination (100 mW cm^{-2}).

TA (°C)	V_{oc} (V)	J_{sc} (mA/cm^2)	FF (%)	PCE (%)
80	0.928	26.88	76.81	19.16
90	0.933	26.95	77.26	19.42
100	0.929	27.26	76.22	19.32
110	0.929	27.06	75.97	19.10

Table S9. Detailed photovoltaic parameters of the PM6:CH-PHE-based devices by optimal conditions under the illumination of AM 1.5 G, 100 mW cm^{-2}.

Active layer	V_{OC} (V)	J_{SC} (mA cm^{-2})	FF (%)	PCE (%)
PM6:CH-PHE	0.944	21.91	73.52	15.20
	0.948	21.87	73.29	15.19
	0.945	21.84	73.49	15.17
	0.954	21.74	72.44	15.02
	0.943	21.58	73.56	14.96
	0.950	21.91	71.76	14.94
	0.956	21.30	73.38	14.94
	0.947	21.35	73.78	14.92
	0.950	21.78	72.07	14.91
	0.944	21.69	72.72	14.89
	0.944	21.99	71.24	14.79
	0.958	21.66	70.96	14.77
	0.953	21.50	70.83	14.56
	0.952	21.30	71.08	14.47
	0.952	21.38	70.43	14.39
	0.944	21.44	70.33	14.29
	0.950	21.33	69.98	14.24
	0.949	21.53	69.33	14.22
	0.948	21.51	69.27	14.18
	0.949	21.59	68.81	14.15
Average	0.949	21.61	71.61	14.71

Table S10. Detailed photovoltaic parameters of the PM6:CH-Bzq-based devices by optimal conditions under the illumination of AM 1.5 G, 100 mW cm^{-2}.

Active layer	V_{OC} (V)	J_{SC} (mA cm^{-2})	FF (%)	PCE (%)
PM6:CH-Bzq	0.957	25.05	69.70	16.71
	0.962	24.82	69.66	16.69
	0.953	24.70	70.70	16.64
	0.953	24.56	71.06	16.63
	0.962	24.84	69.30	16.61
	0.953	24.24	71.50	16.53
	0.955	24.49	70.63	16.52
	0.953	24.43	70.86	16.50
	0.952	24.43	70.94	16.49
	0.956	24.35	70.35	16.43
	0.952	24.32	70.97	16.42
	0.954	24.51	70.19	16.41
	0.954	24.11	70.98	16.39
	0.957	24.27	69.89	16.29
	0.953	24.40	69.83	16.29
	0.956	24.21	70.23	16.25
	0.954	24.24	70.11	16.21
	0.956	23.96	70.79	16.21
	0.954	23.96	70.16	16.04
	0.957	24.38	67.92	15.90
Average	0.955	24.41	70.29	16.41

Table S11. Detailed photovoltaic parameters of the PM6:CH-Bzq-Br-based devices by optimal conditions under the illumination of AM 1.5 G, 100 mW cm^{-2}.

Active layer	V_{OC} (V)	J_{SC} (mA cm^{-2})	FF (%)	PCE (%)
PM6:CH-Bzq-Br	0.933	26.95	77.26	19.42
	0.926	27.10	77.09	19.35
	0.929	27.19	76.46	19.34
	0.926	27.26	76.62	19.34
	0.929	27.26	76.22	19.32
	0.926	27.28	76.39	19.30
	0.931	26.96	76.48	19.21
	0.930	26.86	76.91	19.21
	0.932	27.20	75.67	19.19
	0.928	26.88	76.81	19.17
	0.927	27.02	76.56	19.17
	0.928	27.12	76.01	19.16
	0.925	27.25	75.92	19.15
	0.928	27.23	75.71	19.15
	0.930	27.25	75.56	19.15
	0.931	26.86	76.22	19.12
	0.930	26.84	76.49	19.11
	0.930	26.74	76.80	19.11
	0.928	27.10	75.97	19.10
	0.924	27.44	75.31	19.10
Average	0.929	27.09	76.32	19.21

Table S12. Detailed photovoltaic parameters of the PM6:CH-Bzq-Br in *o*-xy-based devices by optimal conditions processed with ortho-xylene under the illumination of AM 1.5 G, 100 mW cm^{-2}.

Active layer	V_{OC} (V)	J_{SC} (mA cm^{-2})	FF (%)	PCE (%)
PM6:CH-Bzq-Br in o-xy	0.920	27.04	75.94	18.89
	0.918	27.12	75.86	18.88
	0.911	27.23	75.98	18.86
	0.916	26.82	76.50	18.80
	0.919	26.71	76.45	18.78
	0.917	27.13	75.45	18.77
	0.917	26.76	76.47	18.77
	0.911	27.43	75.12	18.76
	0.909	27.43	74.92	18.67
	0.914	26.80	76.18	18.65
	0.922	26.51	76.23	18.63
	0.921	26.91	75.16	18.63
	0.918	26.81	75.69	18.62
	0.916	26.75	75.89	18.60
	0.913	26.83	75.84	18.58
	0.909	27.34	74.63	18.56
	0.911	27.10	75.03	18.52
	0.916	26.54	76.11	18.52
	0.910	26.99	75.36	18.50
	0.908	27.24	74.75	18.50
Average	0.915	26.97	75.68	18.67

Table S13. Photovoltaic performances of small-area binary OSCs summary with PCEs over 16% processed by non-halogenated solvent.

Active layer	Solvent	V_{oc} (V)	J_{sc} (mA cm^{-2})	FF (%)	PCE (%)	Ref.
T1:BTP-4F-12	THF	0.853	25.2	75.0	16.1	3
PM6:DTY6	o-xy	0.856	24.94	75.5	16.1	4
PM6-Ir1.5:Y6-C2	Tol	0.842	26.23	74.80	16.52	5
PTzBI-*d*F:BTP-Th	o-xy	0.863	25.7	75.4	16.7	6
PTzBI-*d*F:BTP-TBr	o-xy	0.845	27.5	78.8	18.3	
PM6:L8-Ph	o-xy	0.870	26.40	80.11	18.40	7
PM6:YSe-C6	o-xy	0.85	25.94	73.0	16.11	8
PM6:BTP-EHBO-4F	o-xy	0.85	26.12	75.78	16.82	9
D18:BTP-eC9-4F	o-xy	0.827	26.10	74.95	16.18	10
PM6:BO-4Cl	o-xy	0.847	26.86	79.63	18.12	11
PM6:BTP-eC9	o-xy	0.847	27.22	80.31	18.52	
PM1:L8-BO	THF	0.877	26.2	77.1	17.7	12
	Tol	0.887	26.4	77.2	18.1	
JD40-BDD20:PJTVT	o-xy	0.91	23.88	75.54	16.35	13
PM6:G-Trimer	o-xy	0.896	26.75	79.30	19.01	14
PM6:PY-82	o-xy	0.942	23.60	76.1	16.92	15
PM6:Y6-HU	o-xy	0.87	25.6	77.9	17.4	16
PM6:Y6-BO	o-xy	0.832	27.3	78.4	17.8	17
PM6:L8-BO	o-xy	0.858	25.10	77.8	16.75	18
PQM-Cl:PY-IT	Tol	0.920	24.3	80.7	18.0	19
PM6:eC11	o-xy	0.846	26.23	77.3	17.15	20
PBDB-TF:BTIC-2Cl-γCF$_3$	Tol	0.84	25.09	76.99	16.31	21
D18-Cl:BTP-2T	Tol	0.890	24.83	75.4	16.66	22
D18-Cl:BTP-T	Tol	0.847	26.87	76.5	17.07	
D18-Cl:BTP-T-BO	Tol	0.917	24.75	79.5	18.05	
PBQx-TCl:FM24-Cl	o-xy	0.905	25.66	78.85	18.30	23
PBQx-TCl:MM24-Cl	o-xy	0.911	25.13	75.84	17.35	
PM6:PY-V-γ	Tol	0.906	24.5	76.4	17.0	24

PM6:NA3	o-xy	0.906	26.94	77.6	18.94	[25]
PM6:BTP-eC9	Tol	0.87	25.7	76.7	17.1	[26]
	DBE	0.86	28.0	80.5	19.4	
PM6:CH-Bzq-Br	***o*-xy**	**0.920**	**27.04**	**75.94**	**18.89**	**This work**

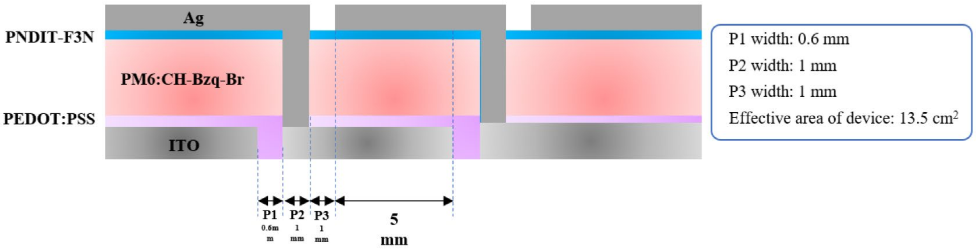

P1 width: 0.6 mm
P2 width: 1 mm
P3 width: 1 mm
Effective area of device: 13.5 cm^2

Figure S40. Schematic diagram of the large-area modules.

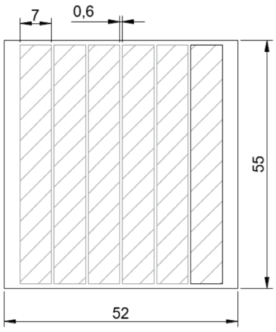

Figure S41. A top-view schematic of the large-area OSC module architecture consisting of six sub-cells connected in series.

Table S14. Photovoltaic performances of large-area OPV modules summary with areas over 10 cm^2.

Active layer	Area (cm^2)	Solvent	PCE (%)	Ref
PM6:G-Trimer	46.2	o-xy	13.25	[14]
PM6:L8-BO:BTO-BO	15.03	Tol	16.35	[27]
PM6:Qx-1	30	o-xy	12.21	[28]
PM6:PY-82:PY-DT	16.5	o-xy	13.84	[15]
PM6:BTP-eC9	25.21	Tol	14.07	[29]
PM6:Y6:20% BTO:PC$_{71}$BM	36	paraxylene	14.26	[30]
PM6:DTY6	18.05	o-xy	14.4	[4]
PM6:CH7	25.2	o-xy	14.42	[31]
PM6:BTP-BO-4Cl	18.73	Tol	14.79	[32]
PM6:L8-BO	18.73	Tol	15.2	[33]
D18:DTC11	21	CS$_2$+o-xylene	15.4	[34]
PBDB-T-2F:BTP-	10.1	CHCl$_3$	12.6	[35]

eC9:$PC_{71}BM$				
PM6:Y6:$PC_{71}BM$	54	CF+CN	13.2	
PM6:Y6:ITIC:$PC_{71}BM$	19.34	CF	13.25	36
PM6:Y6:$PC_{60}BM$	26.2	CF	12.67	37
PM6:BTP-4Cl-12	25.42	CB	12.42	38
PM6:Y6	36	CF	13.47	39
PM6:L8-BO:BTP-S8:BTP-S2	72.25	Tol	12.78	40
PM6:BTP-eC9	16.94	o-xy+MES	14.58	41
PBDB-TFCl:D18-Cl:PY-IT	36.2	CB	15.1	42
PM6:D18:L8-BO	15.64 72	Tol	16.03 14.45	43
PM6:D18:BTP-eC9	15.64	CF	16.70	44
PM6:Y6	28.82	o-xy	12.64	45
PM6:Y6-hu	31.5	o-xy	12.44	46
PTF5:Y6-BO	54.45	o-xy	11.6	47
PM6:P2:Y7-BO	55	o-xy	13.88	48
PBDB-T-2F:N3:P(NDI2OD-T2)	20.61	CF+1-CN	14.31	49
PBDB-T-2F:N3:P(NDI2OD-T2)	58.5	CF+1-CN	14.04	
PB2:FTCC-Br:BTP-eC9	54	CB	15.2	50
PM6:BO-4Cl:m-BTP-PhC6	19.3	CF:1-CN	16.04	51
PM6-PBDBT(55):IPC1CN-BBO-IC2Cl	58.5	CF	11.28	52
PBDB-T-2F:Y6:$PC_{70}BM$	50	CF:1-CN	13.12	53
PM6:PBQx-TCl:PY-IT	19.3	Tol	16.26	54
PM6:BTP-eC9:BTP-S16:BTP-S17	19.3	Tol	15.48	
PM6:BTP-eC9:L8-BO:BTP-S10	72.25	CF	12.20	55
PBQx-TTF:eC9-2Cl	23.6	Tol	16.1	56
PM6:Y7-BO:PC71BM:BTA-ERH	55	CF:CB	12.20	57
D18-Cl:BTP-4F-P2EH	17.6	CF:CB	17.0	58
PM6:CH-Bzq-Br	**13.5**	***o*-xy**	**16.08**	**This work**

Table S15. Detailed energy loss parameters of PM6:CH-PHE, PM6:CH-Bzq, PM6:CH-Bzq-Br and PM6:CH-Bzq-Br in *o*-xy-based optimized devices based on the SQ limit theory.

Active layers	E_g[a] (eV)	V_{oc} (V)	E_{loss}[b] (eV)	V_{oc}^{SQ}[c] (V)	ΔE_1[d] (eV)	V_{oc}^{rad}[e] (V)	ΔE_2[f] (eV)	ΔE_3[g] (eV)	ΔE_3[h] (eV)
PM6:CH-PHE	1.478	0.944	0.534	1.208	0.270	1.114	0.094	0.170	0.188
PM6:CH-Bzq	1.486	0.957	0.529	1.215	0.270	1.140	0.075	0.184	0.195
PM6:CH-Bzq-Br	1.432	0.933	0.499	1.166	0.266	1.106	0.060	0.173	0.193
PM6:CH-Bzq-Br (in *o*-xy)	1.431	0.920	0.511	1.165	0.266	1.116	0.049	0.196	0.202

[a]E_g was estimated via the derivatives of the sensitive EQE (EQE$_{PV}$) spectra. [b]$E_{loss} = E_g - qV_{oc}$. [c]V_{oc}^{SQ} is the upper limit for the V_{oc} of the solar cell derived in the Shockley-Quessier theory. [d]$\Delta E_1 = E_g - qV_{oc}^{SQ}$. [e]$V_{oc}^{rad}$ is the radiative recombination limit for the V_{oc} of the solar cell. [f]$\Delta E_2 = qV_{oc}^{SQ} - qV_{oc}^{rad}$. [g]$\Delta E_3 = E_{loss} - \varDelta E_1 - \varDelta E_2$, [h]$\Delta E_3 = -kT\ln(EQE_{EL})$.

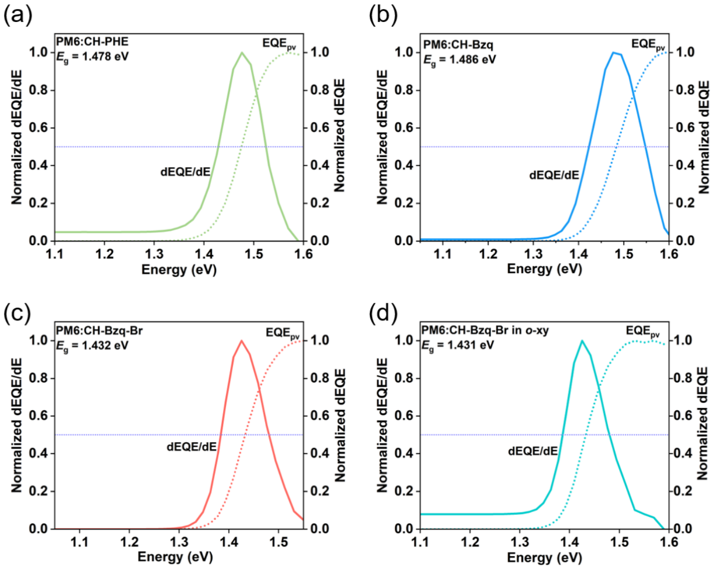

Figure S42. Optical bandgap determination of (a) PM6:CH-PHE, (b) PM6:CH-Bzq, (c) PM6:CH-Bzq-Br and (d) PM6:CH-Bzq-Br in *o*-xy on the basis of the derivatives of the sensitive EQE spectra (*d*EQE/*dE*) for optimized OSCs.

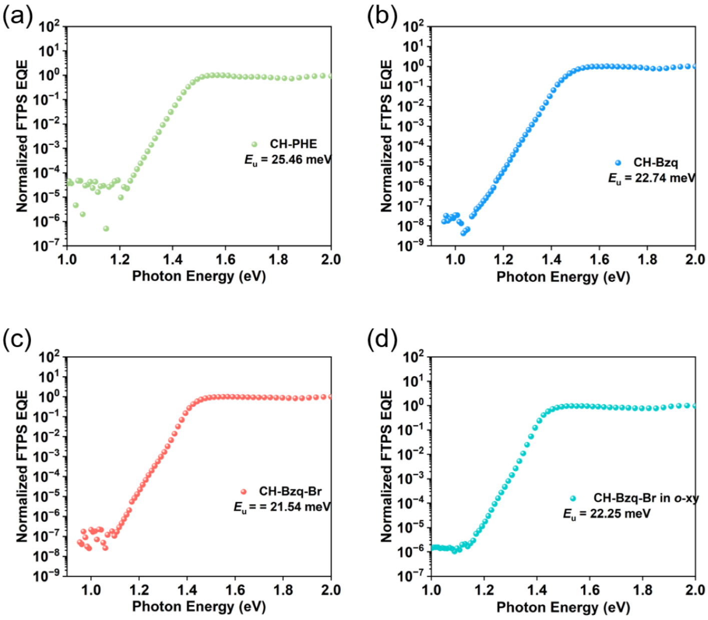

Figure S43. FTPS-EQE spectra for (a) PM6:CH-PHE, (b) PM6:CH-Bzq, (c) PM6:CH-Bzq-Br and (d) PM6:CH-Bzq-Br in *o*-xy-based devices.

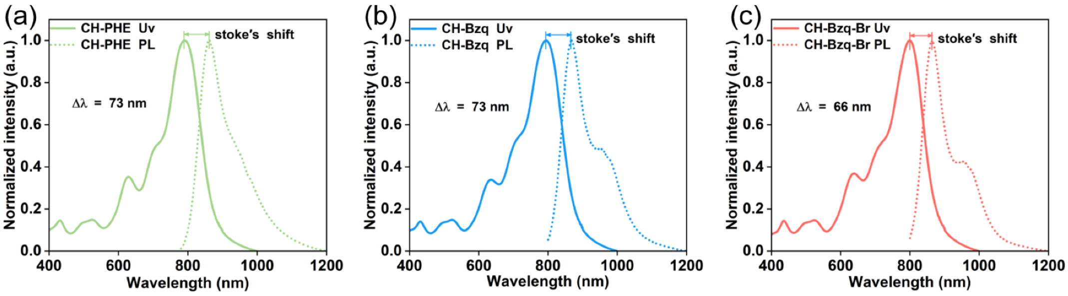

Figure S44. Normalized UV-vis absorption and photoluminescence (PL) spectra of (a) CH-PHE, (b) CH-Bzq and (c) CH-Bzq-Br in the film state.

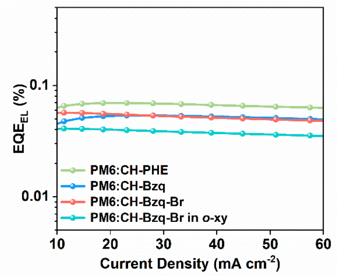

Figure S45. EQE_{EL} spectra for the PM6:CH-PHE, PM6:CH-Bzq, PM6:CH-Bzq-Br and PM6:CH-Bzq-Br in *o*-xy-based devices.

Table S16. Comparison of asymmetric binary OSCs performance and non-radiative energy loss/energy loss between this work and previous work reported in recent years.

Active Layer	V_{oc} (V)	J_{SC} (mA cm^{-2})	FF (%)	PCE (%)	E_{loss}	Ref.
PM6:CH21	0.873	26.57	78.13	18.12	0.525	59
D18:AQx-1F	0.947	24.3	76.9	17.7	0.506	60
D18:AQx-3F	0.946	23.3	75.0	16.5	0.539	
D18:AQx-6	0.892	26.8	77.8	18.6	0.518	61
PM6:BTP-T-3Cl	0.893	26.02	75.79	17.61	0.51	62
PM6:AC9	0.871	26.75	79.0	18.43	0.539	63
PM6:BTP-S9	0.854	27.17	78.6	18.19	0.533	64
PM6:BTP-S2	0.945	24.07	72.02	16.37	0.53	65
PM6:BTP-S8	0.852	26.96	75.45	17.33	0.543	66
PM6:BTP-Cl	0.86	25.79	76.9	17.10	0.54	67
PM6:BTP-2Cl	0.85	25.44	75.6	16.35	0.56	
D18:DT-C8	0.869	27.85	79.6	19.27	0.549	68
D18:DT-C8Cl	0.851	28.17	80.9	19.40	0.556	
D18:DT-C8BTz	0.849	26.75	79.0	17.95	0.562	
PM6:BTP-2F-ThCl	0.869	25.38	77.4	17.06	0.53	69
PM6:asy-YC11	0.849	26.74	72.7	16.52	0.514	70
PM6:bi-asy-YC12	0.871	26.39	74.3	17.16	0.492	
PM1:BTP-2F2Cl	0.861	27.35	78.16	18.40	0.549	71
PM6:NQF	0.921	25.79	73.96	17.57	0.504	72
PM6:C5BTP-BO-2Cl-2F	0.86	25.7	76.5	16.9	0.57	73
PM6:C7BTP-BO-2Cl-2F	0.85	26.7	79.3	18.0	0.56	
PM6:C9BTP-BO-2Cl-2F	0.86	25.9	78.6	17.5	0.55	
PM6:A-C10ch	0.887	26.5	78.1	18.4	0.550	74
PBDB-T:LL3	0.86	26.97	72.27	16.82	0.50	75
PM6:Y-FIC-γe	0.877	25.86	71.85	16.39	0.545	76
PM6:BP4T-4F	0.839	26.3	77.7	17.1	0.550	77
PM6:BP5T-4F	0.888	24.6	76.3	16.7	0.530	
D18:BS3TSe-4F	0.828	29.40	75.94	18.48	0.540	78
D18-Cl:BTP-T	0.847	26.87	76.5	17.07	0.539	22

D18-Cl:BTP-T-BO	0.917	24.75	79.5	18.05	0.542	
PBQx-TCl:FM24-Cl	0.905	25.66	78.85	18.30	0.539	23
MPhS-C2:SSe-NIC	0.876	26.29	73.08	16.83	0.499	79
PM6:CH-Bzq-Br	**0.933**	**26.95**	**77.26**	**19.42**	**0.499**	**This work**
PM6:CH-Bzq-Br in *o*-xy	**0.920**	**27.04**	**75.94**	**18.89**	**0.511**	**This work**

Table S17. Charge carrier transport parameters of the optimized PM6:CH-PHE, PM6:CH-Bzq and PM6:CH-Bzq-Br based devices.

Active layers	μ_e[a] (10^{-4} cm^2 V^{-1} s^{-1})	μ_h[a] (10^{-4} cm^2 V^{-1} s^{-1})	μ_h/μ_e	Slope[b] (kT/q)	α[c]
PM6:CH-PHE	1.57	2.73	1.74	1.432	0.991
PM6:CH-Bzq	1.88	2.96	1.57	1.107	0.993
PM6:CH-Bzq-Br	2.73	3.28	1.20	1.104	0.994

[a] μ_e and μ_h are electron and hole mobilities of the related devices by SCLC measurements. [b] Slope was the slope of V_{oc} versus the natural logarithm of P_{light} obtained from plots of dependence of V_{oc} on P_{light} of optimized OSCs. [c] α was obtained from pots of dependence of J_{sc} on P_{light} of optimized OSCs.

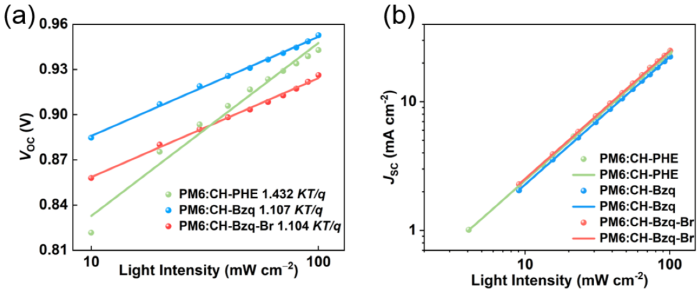

Figure S46. (a) Open-circuit voltage (V_{oc}) and (b) short-circuit current density (J_{sc}) versus light intensity (P_{light}) curves for PM6:CH-PHE, PM6:CH-Bzq and PM6:CH-Bzq-Br devices.

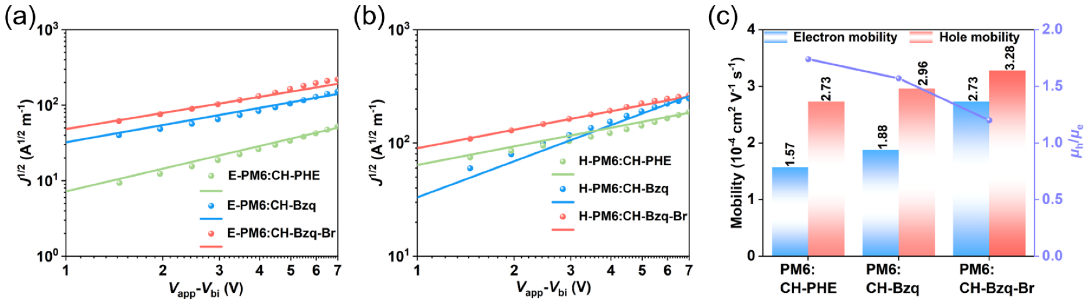

Figure S47. The *J-V* characteristics in dark for (a) electron mobilities and (b) hole mobilities based on PM6:CH-PHE, PM6:CH-Bzq and PM6:CH-Bzq-Br blends. (c) Histograms of the hole and electron mobility for the three blends acquired from single-carrier devices.

Table S18. Summary of the GIWAXS parameters for the pristine CH-PHE, CH-Bzq and CH-Bzq-Br films.

Materials	(010) Diffraction Peak				(100) Diffraction Peak			
	q (Å^{-1})	d[a] (Å)	FWHM (Å^{-1})	CCL[b] (Å)	q (Å^{-1})	d[a] (Å)	FWHM (Å^{-1})	CCL[b] (Å)
CH-PHE	1.673	3.75	0.271	20.86	0.280	22.43	0.061	92.66
CH-Bzq	1.685	3.73	0.255	22.16	0.275	22.84	0.075	75.36
CH-Bzq-Br	1.690	3.71	0.238	23.75	0.277	22.67	0.067	84.36

[a]Calculated from the equation: d-spacing=2π/q. [b]Obtained from the Scherrer equation: CCL= 2πK/FWHM, where FWHM is the full-width at half-maximum and K is a shape factor (K= 0.9 here).

Table S19. Summary of the GIWAXS parameters for the PM6:CH-PHE, PM6:CH-Bzq and PM6:CH-Bzq-Br blend films.

Materials	(010) Diffraction Peak				(100) Diffraction Peak			
	q (Å^{-1})	d[a] (Å)	FWHM (Å^{-1})	CCL[b] (Å)	q (Å^{-1})	d[a] (Å)	FWHM (Å^{-1})	CCL[b] (Å)
PM6:CH-PHE	1.660	3.78	0.251	22.52	0.295	21.29	0.051	110.82
PM6:CH-Bzq	1.732	3.62	0.237	23.85	0.293	21.43	0.042	134.57
PM6:CH-Bzq-Br	1.723	3.64	0.229	24.68	0.288	21.80	0.045	125.60

[a]Calculated from the equation: d-spacing=2π/q. [b]Obtained from the Scherrer equation: CCL=

2πK/FWHM, where FWHM is the full-width at half-maximum and K is a shape factor (K= 0.9 here).

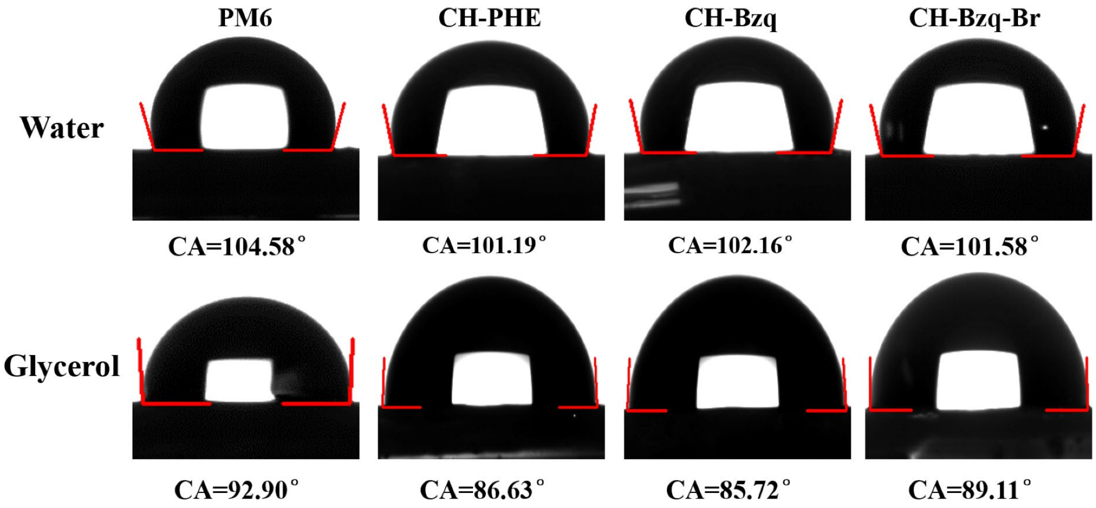

Figure S48. The images of water and glycerol droplet contact angles for PM6, CH-PHE, CH-Bzq and CH-Bzq-Br neat films.

Table S20. Information about surface energies of PM6, CH-PHE, CH-Bzq and CH-Bzq-Br neat films calculated by water and glycerol contact angle.

Materials	θ_{water} (°)	$\theta_{glycerol}$ (°)	γ_d (mN m^{-1})	γ_p (mN m^{-1})	γ (mN m^{-1})	$\chi_{D:A}$ [a] (K)
PM6	104.58	92.90	27.69	0.14	27.83	-
CH-PHE	101.19	86.63	34.14	0.08	34.22	0.33
CH-Bzq	102.16	85.72	33.61	0.05	33.66	0.28
CH-Bzq-Br	101.58	89.11	31.66	0.16	31.82	0.13

[a]The molecular miscibility can be evaluated by Flory–Huggins interaction parameter χ, which is calculated by using the equation of: $\chi_{D:A} = K(\sqrt{\gamma_D} - \sqrt{\gamma_A})^2$.

References

1. H. Chen, Y. Zou, H. Liang, T. He, X. Xu, Y. Zhang, Z. Ma, J. Wang, M. Zhang, Q. Li, C. Li, G. Long, X. Wan, Z. Yao and Y. Chen, *Sci. China Chem.* , 2022, **65**, 1362-1373.
2. T. Sainuddin, J. McCain, M. Pinto, H. Yin, J. Gibson, M. Hetu and S. A. McFarland, *Inorg. Chem.* , 2016, **55**, 83-95.
3. L. Hong, H. Yao, Z. Wu, Y. Cui, T. Zhang, Y. Xu, R. Yu, Q. Liao, B. Gao, K. Xian, H. Y. Woo, Z. Ge and J. Hou, *Adv. Mater.* , 2019, **31**, 1903441.
4. S. Dong, T. Jia, K. Zhang, J. Jing and F. Huang, *Joule*, 2020, **4**, 2004-2016.
5. R. Sun, T. Wang, Z. Luo, Z. Hu, F. Huang, C. Yang and J. Min, *Sol. RRL*, 2020, **4**, 2000156.
6. B. Fan, W. Gao, X. Wu, X. Xia, Y. Wu, F. R. Lin, Q. Fan, X. Lu, W. J. Li, W. Ma and A. K. Y. Jen, *Nat. Commun.*, 2022, **13**, 5946.
7. X. Wu, X. Jiang, X. Li, J. Zhang, K. Ding, H. Zhuo, J. Guo, J. Li, L. Meng, H. Ade and Y. Li, *Adv. Mater.* , 2023, **35**, 2302946.
8. C. Kim, S. Chen, J. S. Park, G.-U. Kim, H. Kang, S. Lee, T. N.-L. Phan, S.-K. Kwon, Y.-H. Kim and B. J. Kim, *J. Mater. Chem. A* 2021, **9**, 24622-24630.
9. Y.-J. Su, H. Nie, C.-F. Chang, S.-C. Huang, Y.-H. Huang, T.-W. Chen, K.-K. Hsu, T.-Y. Lee, H.-M. Shih, C.-W. Ko, J.-T. Chen and C.-S. Hsu, *ACS Appl. Mater. Interfaces* 2021, **13**, 59043-59050.
10. H. Lu, G. Ran, Y. Liu, Z. Pei, W. Liu, Y. Liu, Z. Tang, W. Zhang and Z. Bo, *Adv. Funct. Mater.*, 2023, **33**, 2301866.
11. C. Yang, M. Jiang, S. Wang, B. Zhang, P. Mao, H. Y. Woo, F. Zhang, J.-l. Wang and Q. An, *Adv. Mater.* , 2024, **36**, 2305356.
12. J. Wan, Y. Wu, R. Sun, J. Qiao, X. Hao and J. Min, *Energy Environ. Sci.*, 2022, **15**, 5192-5201.
13. J. Zhang, Q. Huang, K. Zhang, T. Jia, J. Jing, Y. Chen, Y. Li, Y. Chen, X. Lu, H. Wu, F. Huang and Y. Cao, *Energy Environ. Sci.*, 2022, **15**, 4561-4571.
14. C. Wang, X. Ma, Y.-f. Shen, D. Deng, H. Zhang, T. Wang, J. Zhang, J. Li, R. Wang, L. Zhang, Q. Cheng, Z. Zhang, H. Zhou, C. Tian and Z. Wei, *Joule*, 2023, **7**, 2386-2401.
15. Y. Cai, C. Xie, Q. Li, C. Liu, J. Gao, M. H. Jee, J. Qiao, Y. Li, J. Song, X. Hao, H. Y. Woo, Z. Tang, Y. Zhou, C. Zhang, H. Huang and Y. Sun, *Adv. Mater.* , 2023, **35**, 2208165.
16. Z. Abbas, S. U. Ryu, M. Haris, C. E. Song, H. K. Lee, S. K. Lee, W. S. Shin, T. Park and J.-C. Lee, *Nano Energy*, 2022, **101**, 107574.
17. J. Jing, S. Dong, K. Zhang, B. Xie, J. Zhang, Y. Song and F. Huang, *Nano Energy*, 2022, **93**, 106814.
18. R. Ma, X. Jiang, J. Fu, T. Zhu, C. Yan, K. Wu, P. Müller-Buschbaum and G. Li, *Energy Environ. Sci.*, 2023, **16**, 2316-2326.
19. J. Wang, Y. Cui, Y. Xu, K. Xian, P. Bi, Z. Chen, K. Zhou, L. Ma, T. Zhang, Y. Yang, Y. Zu, H. Yao, X. Hao, L. Ye and J. Hou, *Adv. Mater.* , 2022, **34**, 2205009.
20. R. Ma, C. Yan, P. W.-K. Fong, J. Yu, H. Liu, J. Yin, J. Huang, X. Lu, H. Yan and G. Li, *Energy Environ. Sci.*, 2022, **15**, 2479-2488.
21. H. Chen, H. Lai, Z. Chen, Y. Zhu, H. Wang, L. Han, Y. Zhang and F. He, *Angew. Chem. Int. Ed.* , 2021, **60**, 3238-3246.
22. X. Jiang, H. Yang, S. Shen, Y. Wu, C. Cui and Y. Li, *Adv. Funct. Mater.*, 2024, **34**, 2409723.
23. Y. Gong, T. Zou, X. Li, S. Qin, G. Sun, T. Liang, R. Zhou, J. Zhang, J. Zhang, L. Meng, Z. Wei

and Y. Li, *Energy Environ. Sci.*, 2024, **17**, 6844-6855.

24. C. Zhao, L. Wang, G. Zhang, Y. Wang, R. Hu, H. Huang, M. Qiu, S. Li and G. Zhang, *Molecules*, 2022, **27**, 5739.
25. Z. Luo, W. Wei, R. Ma, G. Ran, M. H. Jee, Z. Chen, Y. Li, W. Zhang, H. Y. Woo and C. Yang, *Adv. Mater.* , 2024, **36**, 2407517.
26. S. Gao, Y. Zhang, S. Jeong, X. Zhou, H. Xu, S. Xu, D. Chen, W. Liu, C. Yang, S. Meng, W. Zhu and X. Song, *Energy Environ. Sci.*, 2024, **17**, 5542-5551.
27. H. Chen, W. Sun, R. Zhang, Y. Huang, B. Zhang, G. Zeng, J. Ding, W. Chen, F. Gao, Y. Li and Y. Li, *Adv. Mater.* , 2024, **36**, 2402350.
28. Y.-F. Shen, H. Zhang, J. Zhang, C. Tian, Y. Shi, D. Qiu, Z. Zhang, K. Lu and Z. Wei, *Adv. Mater.* , 2023, **35**, 2209030.
29. X. Dong, Y. Jiang, L. Sun, F. Qin, X. Zhou, X. Lu, W. Wang and Y. Zhou, *Adv. Funct. Mater.*, 2022, **32**, 2110209.
30. H. Chen, R. Zhang, X. Chen, G. Zeng, L. Kobera, S. Abbrent, B. Zhang, W. Chen, G. Xu, J. Oh, S.-H. Kang, S. Chen, C. Yang, J. Brus, J. Hou, F. Gao, Y. Li and Y. Li, *Nat. Energy*, 2021, **6**, 1045-1053.
31. S. Zhang, H. Chen, P. Wang, S. Li, Z. Li, Y. Huang, J. Liu, Z. Yao, C. Li, X. Wan and Y. Chen, *Sol. RRL*, 2023, **7**, 2300029.
32. J.-Y. Fan, Z.-X. Liu, J. Rao, K. Yan, Z. Chen, Y. Ran, B. Yan, J. Yao, G. Lu, H. Zhu, C.-Z. Li and H. Chen, *Adv. Mater.* , 2022, **34**, 2110569.
33. J. Xiang, Z.-X. Liu, H. Chen and C.-Z. Li, *Adv. Mater.* , 2023, **35**, 2303729.
34. Z. Zhong, S. Chen, J. Zhao, J. Xie, K. Zhang, T. Jia, C. Zhu, J. Jing, Y. Liang, L. Hong, S. Zhu, D. Ma and F. Huang, *Adv. Energy Mater.* , 2023, **13**, 2302273.
35. F. Qin, L. Sun, H. Chen, Y. Liu, X. Lu, W. Wang, T. Liu, X. Dong, P. Jiang, Y. Jiang, L. Wang and Y. Zhou, *Adv. Mater.* , 2021, **33**, 2103017.
36. Z. Jia, Z. Chen, X. Chen, J. Yao, B. Yan, R. Sheng, H. Zhu and Y. Yang, *Photonics Res.* , 2021, **9**, 324-330.
37. A. Distler, C. J. Brabec and H.-J. Egelhaaf, *Prog Photovolt.* , 2021, **29**, 24-31.
38. Y. Han, Z. Hu, W. Zha, X. Chen, L. Yin, J. Guo, Z. Li, Q. Luo, W. Su and C.-Q. Ma, *Adv. Mater.* , 2022, **34**, 2110276.
39. B. Zhang, F. Yang, S. Chen, H. Chen, G. Zeng, Y. Shen, Y. Li and Y. Li, *Adv. Funct. Mater.*, 2022, **32**, 2202011.
40. X. Kong, L. Zhan, S. Li, S. Yin, H. Qiu, Y. Fu, X. Lu, Z. Chen, H. Zhu, W. Fu and H. Chen, *Chem. Eng. J.* , 2023, **473**, 145201.
41. H. Wang, S. Liu, H. Li, M. Li, X. Wu, S. Zhang, L. Ye, X. Hu and Y. Chen, *Adv. Mater.* , 2024, **36**, 2313098.
42. J. Wang, Y. Wang, K. Xian, J. Qiao, Z. Chen, P. Bi, T. Zhang, Z. Zheng, X. Hao, L. Ye, S. Zhang and J. Hou, *Adv. Mater.* , 2024, **36**, 2305424.
43. B. Zhang, W. Chen, H. Chen, G. Zeng, R. Zhang, H. Li, Y. Wang, X. Gu, W. Sun, H. Gu, F. Gao, Y. Li and Y. Li, *Energy Environ. Sci.*, 2024, **17**, 2935-2944.
44. H. Gu, J. Zhu, H. Chen, G. Zeng, X. Chen, X. Tang, J. Xia, T. Zhang, B. Zhang, J. Zhang, J. Ding, Y. Li and Y. Li, *Giant*, 2024, **18**, 100286.
45. Y. Li, J. Wu, X. Yi, Z. Liu, H. Liu, Y. Fu, J. Liu and Z. Xie, *J. Mater. Chem. C* 2023, **11**, 13263-13273.

46. S. Rasool, J. W. Kim, H. W. Cho, Y.-J. Kim, D. C. Lee, C. B. Park, W. Lee, O.-H. Kwon, S. Cho and J. Y. Kim, *Adv. Energy Mater.* , 2023, **13**, 2203452.
47. Z. U. Rehman, M. Haris, S. U. Ryu, M. Jahankhan, C. E. Song, H. K. Lee, S. K. Lee, W. S. Shin, T. Park and J.-C. Lee, *Adv. Sci.* , 2023, **10**, 2302376.
48. T. Gokulnath, H. Kim, J. Lee, B. H. Cho, H.-Y. Park, J. Jee, Y. Y. Kim, K. Kranthiraja, J. Yoon and S.-H. Jin, *Adv. Energy Mater.* , 2023, **13**, 2302538.
49. S. Yoon, S. Park, S. H. Park, S. Nah, S. Lee, J.-W. Lee, H. Ahn, H. Yu, E.-Y. Shin, B. J. Kim, B. K. Min, J. H. Noh and H. J. Son, *Joule*, 2022, **6**, 2406-2422.
50. J. Wang, P. Bi, Y. Wang, Z. Zheng, Z. Chen, J. Qiao, W. Wang, J. Li, C. An, S. Zhang, X. Hao and J. Hou, *CCS Chem.* , 2023, **6**, 218-229.
51. D. Wang, Y. Li, G. Zhou, E. Gu, R. Xia, B. Yan, J. Yao, H. Zhu, X. Lu, H.-L. Yip, H. Chen and C.-Z. Li, *Energy Environ. Sci.*, 2022, **15**, 2629-2637.
52. P. Gopikrishna, J. Rhee, S. Yoon, D. Um, H. Jin, Y. Jun, H. Choi, H. J. Son and B. Kim, *Adv. Funct. Mater.*, 2023, **33**, 2305541.
53. M. Jahandar, A. Prasetio, C. Lee, H. Kim, A. R. Kim, J. Heo, Y. Kim, S. Kim and D. C. Lim, *Chem. Eng. J.* , 2022, **448**, 137555.
54. T. Chen, X. Zheng, D. Wang, Y. Zhu, Y. Ouyang, J. Xue, M. Wang, S. Wang, W. Ma, C. Zhang, Z. Ma, S. Li, L. Zuo and H. Chen, *Adv. Mater.* , 2024, **36**, 2308061.
55. L. Zhan, S. Yin, Y. Li, S. Li, T. Chen, R. Sun, J. Min, G. Zhou, H. Zhu, Y. Chen, J. Fang, C.-Q. Ma, X. Xia, X. Lu, H. Qiu, W. Fu and H. Chen, *Adv. Mater.* , 2022, **34**, 2206269.
56. J. Wang, Y. Wang, P. Bi, Z. Chen, J. Qiao, J. Li, W. Wang, Z. Zheng, S. Zhang, X. Hao and J. Hou, *Adv. Mater.* , 2023, **35**, 2301583.
57. T. Gokulnath, J. Kim, H. Kim, J. Park, D. Song, H.-Y. Park, R. Kumaresan, Y. Y. Kim, J. Yoon and S.-H. Jin, *ACS Appl. Mater. Interfaces*, 2023, **15**, 19307-19318.
58. L. Zhu, M. Zhang, G. Zhou, Z. Wang, W. Zhong, J. Zhuang, Z. Zhou, X. Gao, L. Kan, B. Hao, F. Han, R. Zeng, X. Xue, S. Xu, H. Jing, B. Xiao, H. Zhu, Y. Zhang and F. Liu, *Joule*, 2024, **8**, 3153-3168.
59. H. Liang, X. Bi, H. Chen, T. He, Y. Lin, Y. Zhang, K. Ma, W. Feng, Z. Ma, G. Long, C. Li, B. Kan, H. Zhang, O. A. Rakitin, X. Wan, Z. Yao and Y. Chen, *Nat. Commun.*, 2023, **14**, 4707.
60. K. Liu, Y. Jiang, G. Ran, F. Liu, W. Zhang and X. Zhu, *Joule*, 2024, **8**, 835-851.
61. Y. Jiang, Y. Li, F. Liu, W. Wang, W. Su, W. Liu, S. Liu, W. Zhang, J. Hou, S. Xu, Y. Yi and X. Zhu, *Nat. Commun.*, 2023, **14**, 5079.
62. Y. Pan, X. Zheng, J. Guo, Z. Chen, S. Li, C. He, S. Ye, X. Xia, S. Wang, X. Lu, H. Zhu, J. Min, L. Zuo, M. Shi and H. Chen, *Adv. Funct. Mater.* , 2022, **32**, 2108614.
63. C. He, Z. Bi, Z. Chen, J. Guo, X. Xia, X. Lu, J. Min, H. Zhu, W. Ma, L. Zuo and H. Chen, *Adv. Funct. Mater.*, 2022, **32**, 2112511.
64. C. He, Q. Shen, B. Wu, Y. Gao, S. Li, J. Min, W. Ma, L. Zuo and H. Chen, *Adv. Energy Mater.*, 2023, **13**, 2204154.
65. S. Li, L. Zhan, Y. Jin, G. Zhou, T.-K. Lau, R. Qin, M. Shi, C.-Z. Li, H. Zhu, X. Lu, F. Zhang and H. Chen, *Adv. Mater.* , 2020, **32**, 2001160.
66. S. Li, L. Zhan, N. Yao, X. Xia, Z. Chen, W. Yang, C. He, L. Zuo, M. Shi, H. Zhu, X. Lu, F. Zhang and H. Chen, *Nat. Commun.*, 2021, **12**, 4627.
67. Y. Cui, P. Zhu, H. Hu, X. Xia, X. Lu, S. Yu, H. Tempeld, R.-A. Eichel, X. Liao and Y. Chen, *Angew. Chem. Int. Ed.* , 2023, **62**, e202304931.

68. S. Chen, S. Zhu, L. Hong, W. Deng, Y. Zhang, Y. Fu, Z. Zhong, M. Dong, C. Liu, X. Lu, K. Zhang and F. Huang, *Angew. Chem. Int. Ed.* , 2024, **63**, e202318756.
69. Z. Luo, R. Ma, T. Liu, J. Yu, Y. Xiao, R. Sun, G. Xie, J. Yuan, Y. Chen, K. Chen, G. Chai, H. Sun, J. Min, J. Zhang, Y. Zou, C. Yang, X. Lu, F. Gao and H. Yan, *Joule*, 2020, **4**, 1236-1247.
70. Q. Fan, R. Ma, J. Yang, J. Gao, H. Bai, W. Su, Z. Liang, Y. Wu, L. Tang, Y. Li, Q. Wu, K. Wang, L. Yan, R. Zhang, F. Gao, G. Li and W. Ma, *Angew. Chem. Int. Ed.* , 2023, **62**, e202308307.
71. R. Sun, Y. Wu, X. Yang, Y. Gao, Z. Chen, K. Li, J. Qiao, T. Wang, J. Guo, C. Liu, X. Hao, H. Zhu and J. Min, *Adv. Mater.* , 2022, **34**, 2110147.
72. J. Wang, H. Chen, X. Xu, Z. Ma, Z. Zhang, C. Li, Y. Yang, J. Wang, Y. Zhao, M. Zhang, X. Wan, Y. Lu and Y. Chen, *J. Mater. Chem. A* 2022, **10**, 16714-16721.
73. J. Cai, Y. Fu, C. Guo, D. Li, L. Wang, C. Chen, D. Liu, W. Li and T. Wang, *Sci. China Chem.*, 2023, **66**, 508-517.
74. C. Xiao, X. Wang, T. Zhong, R. Zhou, X. Zheng, Y. Liu, T. Hu, Y. Luo, F. Sun, B. Xiao, Z. Liu, C. Yang and R. Yang, *Adv. Sci.* , 2023, **10**, 2206580.
75. H. Lu, H. Jin, H. Huang, W. Liu, Z. Tang, J. Zhang and Z. Bo, *Adv. Funct. Mater.*, 2021, **31**, 2103445.
76. S. Lee, G. Park, M. Jeong, B. Lee, S. Jeong, J. Park, Y. Cho, S. M. Noh and C. Yang, *ACS Appl. Mater. Interfaces*, 2022, **14**, 33614-33625.
77. W. Gao, H. Fu, Y. Li, F. Lin, R. Sun, Z. Wu, X. Wu, C. Zhong, J. Min, J. Luo, H. Y. Woo, Z. Zhu and A. K. Y. Jen, *Adv. Energy Mater.* , 2021, **11**, 2003177.
78. W. Gao, F. Qi, Z. Peng, F. R. Lin, K. Jiang, C. Zhong, W. Kaminsky, Z. Guan, C.-S. Lee, T. J. Marks, H. Ade and A. K. Y. Jen, *Adv. Mater.* , 2022, **34**, 2202089.
79. Y. Gao, X. Yang, W. Wang, R. Sun, J. Cui, Y. Fu, K. Li, M. Zhang, C. Liu, H. Zhu, X. Lu and J. Min, *Adv. Mater.* , 2023, **35**, 2300531.